EML 4905 Senior Design Project

A B.S. THESIS
PREPARED IN PARTIAL FULFILLMENT OF THE
REQUIREMENT FOR THE DEGREE OF
BACHELOR OF SCIENCE
IN
MECHANICAL ENGINEERING

MAGNETOCALORIC TEST BENCH

Francisco Iriarte
Eduardo Garcia
Mikael Liranzo
Advisor: Professor Benjamin Boesl

November 21, 2013

This B.S. thesis is written in partial fulfillment of the requirements in EML 4905. The contents represent the opinion of the authors and not the Department of Mechanical and Materials Engineering.

Ethics Statement and Signatures

The work submitted in this B.S. thesis is solely prepared by a team consisting of Francisco Iriarte, Eduardo Garcia, and Mikael Liranzo and it is original. Excerpts from others' work have been clearly identified, their work acknowledged within the text and listed in the list of references. All of the engineering drawings, computer programs, formulations, design work, prototype development and testing reported in this document are also original and prepared by the same team of students.

Francisco Iriarte	Eduardo Garcia	Mikael Liranzo
Team Leader	Team Member	Team Member

Dr. Benjamin Boesl

Faculty Advisor

Contents

Figures

Tables

1. Abstract

The magnetocaloric effect, also known as MCE, refers to the thermal behavior of certain materials when exposed to a magnetic field. A sample of said material is fixed while a magnetic field is cyclically applied to it. Paired with various heat exchangers, this process produces a refrigeration cycle. The device was designed to serve as a test rig which allowed for easy swapping of the magnetocaloric material. Thermo-fluid analysis of the system, as well as the mechanical design of the apparatus, was performed.

The project was divided into various phases. These phases were design, analysis, and manufacturing. The design portion of the project consists of all rough sketches, calculations, and C.A.D. SolidWorks® was the software of choice for all modeling. Simulations were performed in Solidworks® and ANSYS®. Upon finalizing the design, manufacturing and optimization was performed. Testing of several magnetocaloric alloys was performed to ensure that the device functioned properly.

2. Problem Statement

Current refrigeration cycles are based on processes involving the use of compressed gasses throughout the system. These gasses are known to be harmful to the o-zone layer. Some of the more commonly used blends of these gasses are Hydro-Chlorofluorocarbon (HCFC) and Hydro-fluorocarbon (HFC). MCR (Magnetocaloric Refrigeration) rids itself of the negative effects of HFCs and HCFCs, as this is purely a solid material based operation. The solid will replace the gasses used in classical refrigeration systems, eliminating the aforementioned negative effects. The problem with current MCR systems is the use of liquid helium and liquid nitrogen to cool the solid material when it is passed through a magnetic field. The use of liquid helium and nitrogen renders such system of little use for domestic application. This is due to the danger and high cost of these fluids. The goal is to test various materials, and study their MCE. The acquired data could be used to bring MCR to the domestic market as well as to areas of the world with limited access to energy resources.

3. Motivation

The motivation for studying MCR is mainly due to the current growth in its area of research as well as the possibility of developing an alternative method for refrigeration that does not encourage the use of potentially hazardous materials. This alternative refrigeration system observes environmental awareness and human safety due to the use of non-hazardous ferrous solids as refrigerants. Additionally, marketing a system of this type reveals promise in producing commercial refrigeration units for multipurpose cooling applications. These applications include but are not limited to house-hold refrigeration appliances or heat generating sources for small systems such as water-heaters.

Other than the domestic involvement of MCR, another motive for the study of this process is to obtain various test values for the MCE of any ferrous specimen. The device, through a program medium, will output these test values. This procedure will result in a standardized tabulation of various material properties affected by magnetism that may be used as reference for further study. Ultimately, these values obtained for the tested materials would prove useful to the field of materials engineering.

4. Literary Survey

4.1 About MCR

The principle behind MCR is to be able to use the MCE of a desired material in order to produce a change in temperature (ΔT). This change in temperature is then manipulated by using various heat exchangers in order to produce a refrigeration cycle.

Gadolinium (Gd) has been shown to exhibit higher ΔTs when altering its ambient magnetic field in comparison to other materials that may also exhibit the MCE (V. K. Pecharsky and K. A. Gschneidner, 1997). Magnetocaloric materials, such as Gd, are ideal for such application due to the way that they behave when exposed to a changing magnetic field. Upon exposing the solid to a magnetic field, the magnetic moments within it become aligned. During this process, heat is produced as a byproduct of entropy (H. SZYMCZAK*, 2008). This heat is to be extracted from the material while it is still in the magnetic field. Keeping the sample in the field allows for the magnetic moments to remain aligned. Upon removing the sample from the magnetic field and allowing the moments to become disordered once again, the material will naturally become cooler. At this stage in the cycle, the material will be exposed to a second heat exchanger which will become cool as the material sample attempts to achieve thermal equilibrium. This cold heat exchanger is the one which will potentially serve as the cooling component of a refrigerator.

4.2 Previous Work

An understanding of modern, yet typical, refrigeration systems used in today's commercial applications is necessary before any credibility to the MCR method is given.

Once a heat load is established, the most common idea for the removal of this heat is through the basic and widely accepted thermodynamic cyclic process composed of a compressor, condenser, expansion valve, and evaporator. In series, each of these components function in unison to accomplish the simple task of removing this heat load (i.e. refrigerator). The most general set-up involving the removal of this heat is illustrated through the following figure:

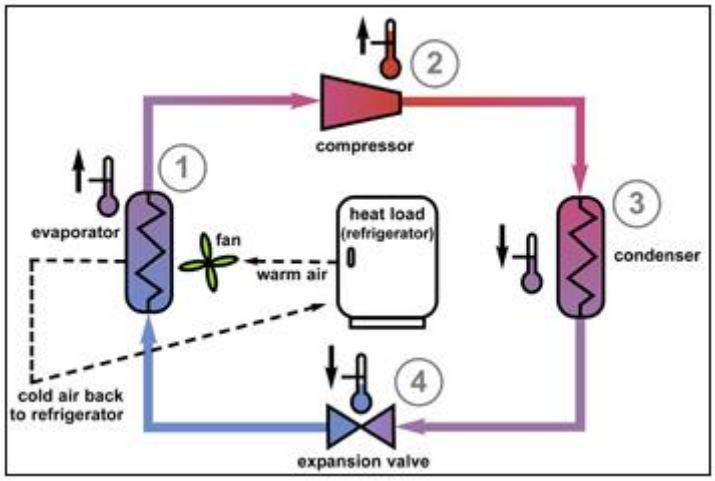

Figure 1: Classical Refrigeration Cycle (D. Liu, 2009)

Within this cycle, there is a working fluid, or refrigerant (usually fluorocarbon based), which allows for the cooling end result. This fluid flows through the compressor causing an increase in temperature due to compression. The condenser removes this heat all while maintaining the current pressure the compressor previously provided. The temperature is then dropped further at the expansion valve due to, as the name implies, expansion. This allows the working fluid to expand and enter the heat load while simultaneously removing the heat stored within through a process of forced convection (fan).

Around the year 1880, a German physicist by the name of Emil Warburg discovered the "cooling by demagnetization" phenomenon. The MCE was, at the time, only discovered by using iron as the test specimen. During 1926 and 1927, adiabatic demagnetization was independently introduced as a thermodynamic process by both Peter Debye and William F. Giauque. The cooling process was experimentally performed by Giauque in 1933 for cryogenic applications, where a temperature drop of .25 Kelvin was achieved. Since then, advancements in this study have been made for industrial sized applications as well as medical purposes.

In 1997, Karl A. Gschneider Jr. at Ames Laboratory developed and first "proof of concept" in-room-temperature MCR process showing a thirty percent improvement in energy efficiency in comparison to previous works in the field. This feat was accomplished through the use of the rare earth metal Gadolinium (Gd) as the refrigerant. The metal, however, was alloyed with other elements such as silicon and germanium in order to produce the maximum amount of MCE

possible. This was also mainly due to feasibility in mass production of the Gd alloy commercial grade compound which only required a small amount of the rare earth metal in the alloying process. This accomplishment also made use of a “permanent” magnet, a new feature which promises the continual use of magnets within the system for continual refrigeration system applications.

4.3 Component Breakdown

4.3.1 Magnets

MCE is achieved in a solid material when it is passed through a magnetic field. The magnetic field most commonly used in industrial and laboratory application is a high magnetic field, which heightens the MCE. When the magnetic field is increased the entropy change is raised, which means the MCE has been increased (D. Baldomir a, 2007). Figure 2 shows that the block temperature shifts to lower values as the magnetic field is increased (D. Baldomir a, 2007).

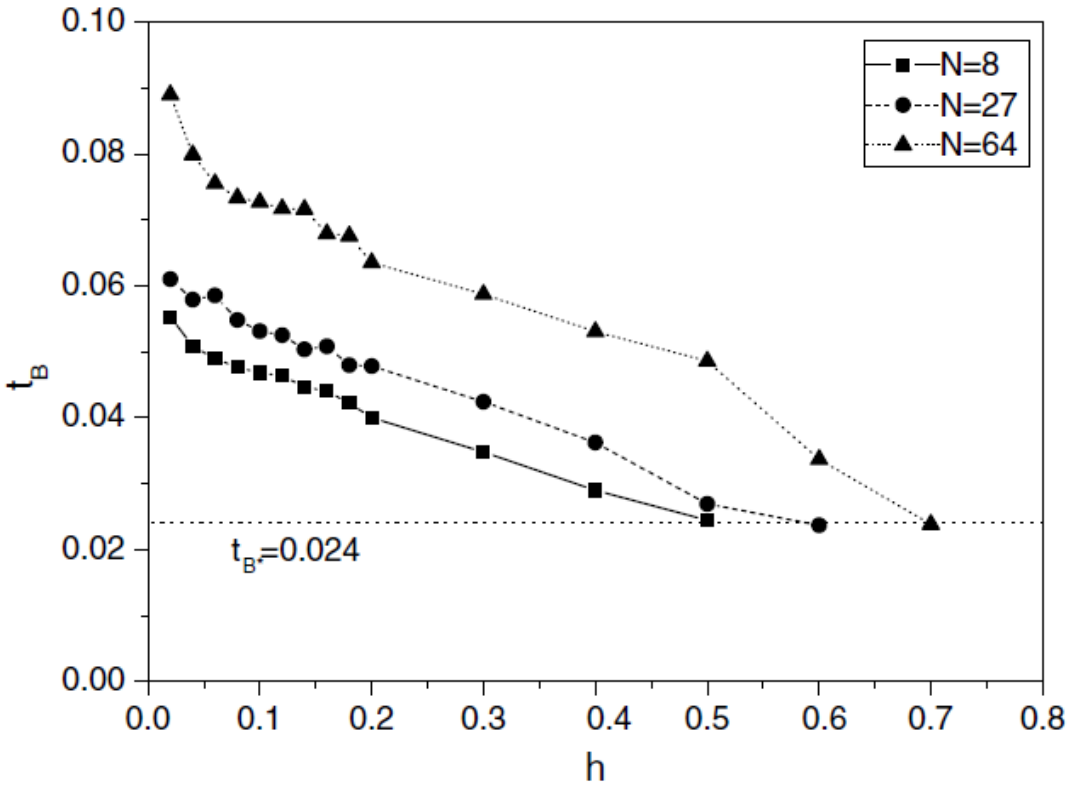

Figure 2: Temperature vs. H (D. Baldomir a, 2007)

Although a higher MCE is achieved, the heat rejection of the solid must be taken into account. The magnet themselves previously used for MCR is a permanent magnet set up or an electromagnet (Bjørk, 2010). An ideal magnet for MCR should have a high magnetic field distributed over the largest volume, while maintaining the minimum amount of magnetic material. The power difference of permanent magnet could be seen in Table 1 according to their composition (LLC, 2007).

Table 1: Properties of Magnets

	Maximum Energy Product *Bhmax(MGOe)*	Residual Flux Density *Br(G)*	Coercive Force *Hc(Koe)*	Working Temperature *°C*
Ceramic 5	3.4	3950	2400	400
Sintered Alnico 5	3.9	10900	620	540
Cast Alnico 8	5.3	8200	1650	540
Samarium Cobalt 20 (1,5)	20	9000	8000	260
Samarium Cobalt 28 (2,17)	28	10500	9500	350
Neodymium N45	45	13500	10800	80
Neodymium 33UH	33	11500	10700	180

Permanent magnets are compact in comparison to electromagnets and do not consume any energy to produce the magnetic field. Electromagnets on the other hands, although a much higher magnetic field can be produced, the consumption of power and its mere size would counter acts its benefits in domestic use. This does not render them useless for MCR, but it would be focused more for the commercial use were component packaging is less of a problem. Permanent magnet would be the magnet of choice for this test rig to reap the benefits of their size and a decent magnetic field.

4.3.2 Heat Exchangers

There are various types of heat exchangers varying in shapes and sizes. The three most common types of heat exchangers are the coil exchanger, plate exchanger and the shell and tube exchanger. The heat exchanger is a critical component of the system as the refrigeration process would not be possible without them.

Figure 3: Coil Heat Exchanger (Bartlett, 1996)

The Coil heat exchanger (See Figure 3) has a very simple design, consisting of a coil made from a small diameter tube that it is concentrically wound around a large tube. The small tube holds the cooling fluid and the large tube holds the working fluid. A coil exchanger is a very inexpensive heat exchanger that is robust and capable of handling very high pressures and temperatures. Although inexpensive, these types of exchanger suffer from poor thermal performance due to the small surface area for heat transfer (Bartlett, 1996).

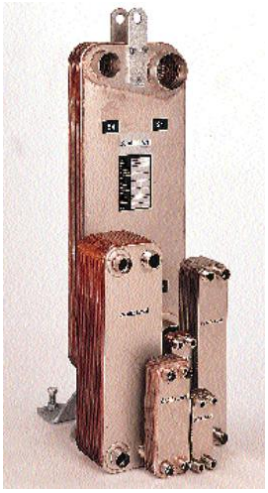

Figure 4: Plate Heat Exchanger (Bartlett, 1996)

Plate heat exchangers are types of heat exchanger that consist of plates with tubes running perpendicular to the plates (See Figure 4). The fluid is pumped through tubes and the plates being very thin and tightly stacked provide a high heat transfer rate due to the high surface

area. This exchanger can only experience low pressure applications in comparison to the coil exchanger. They can withstand about 400°F and 300 psig which is considered a low pressure application (Kevin D. Rafferty, 1992).

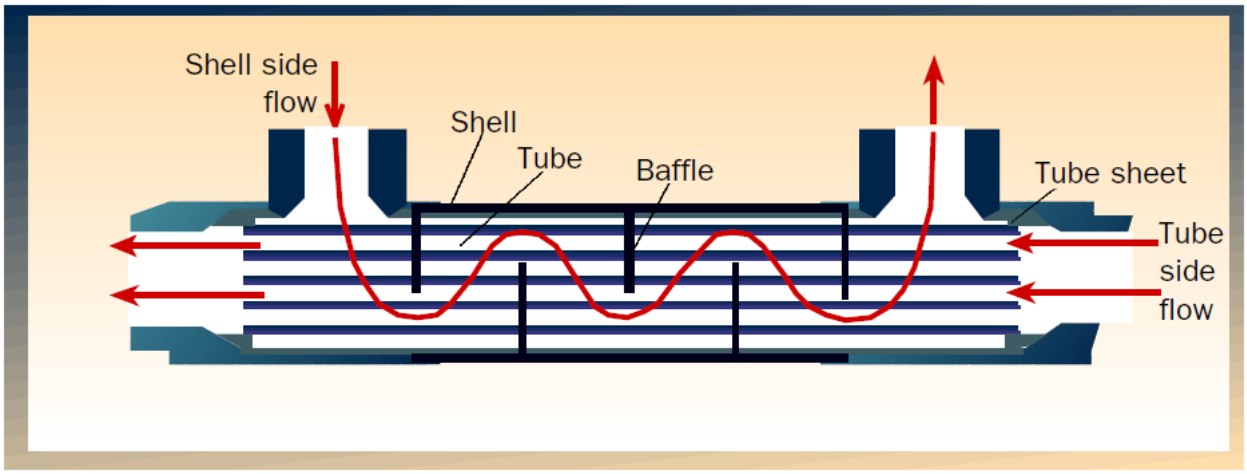

Figure 5: Shell and Tube Heat Exchanger (Bartlett, 1996)

Shell and tube exchanger (See Figure 5) are rather more complex than both the coil and the plate exchanger. Shell and tube exchanger are similar to a plate exchanger, but the stacked fins are enclosed and fluid is pumped through the containing vessel. Such exchangers are the middle ground between the coil and the plate exchangers as they provide higher pressure than the plate exchanger, but not as much as the coil exchanger. The thermal performance is lower values than the plate exchanger, but higher than coil exchangers locating it in the middle ground of the three.

4.3.3 Pumps

Centrifugal pumps operate by creating a pressure head due to an acceleration of the fluid by the impellers. The pressure is increased from the inlet to the outlet though the impellers applying kinetic energy to the fluid and in turn increasing its head. Looked at closer the inner workings of a centrifugal pump and we can see that it is a very simple concept (See Figure 6), but highly effective and inexpensive (Jacobsen, 2002).

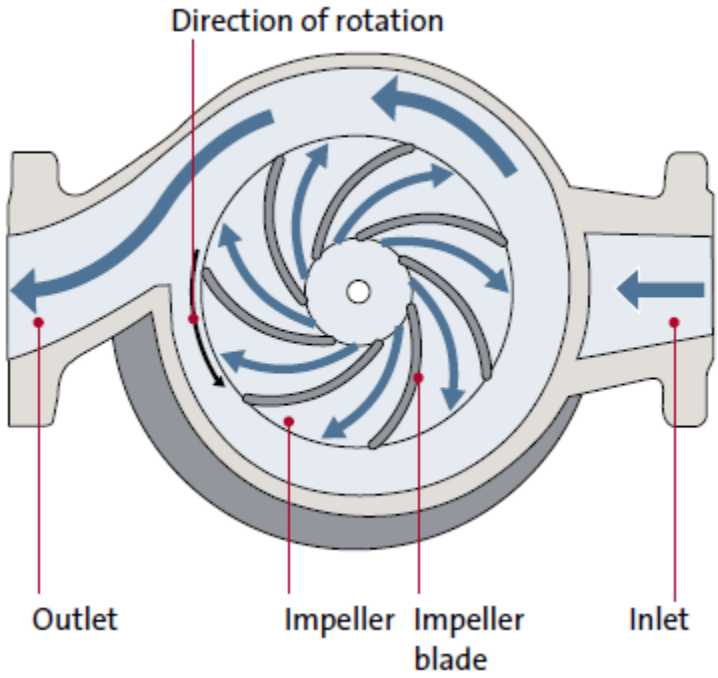

Figure 6: Centrifugal Pump (Jacobsen, 2002)

Centrifugal pumps vary in style such as inline,end suction, double pump and submersible pump. All of these types have the same working principle with slight changes in impeller design, inlet and outlet design, ect. Centrifugal pumps can be addapated to wide range of applications due to this they are very versatile, most likely making it useful for our purpose.

The main difference between a Positive Displacement pump and a centrifugal pump is the operating principle. A Positive Displacement pump creates a flow from inlet to outlet; on the contrary centrifugal pumps create a pressure. A PD pump moves a given volume at suction to discharge it and due to the working principle it maintains a constant volumetric flow in the network at various working pressures (Parker, 1994).

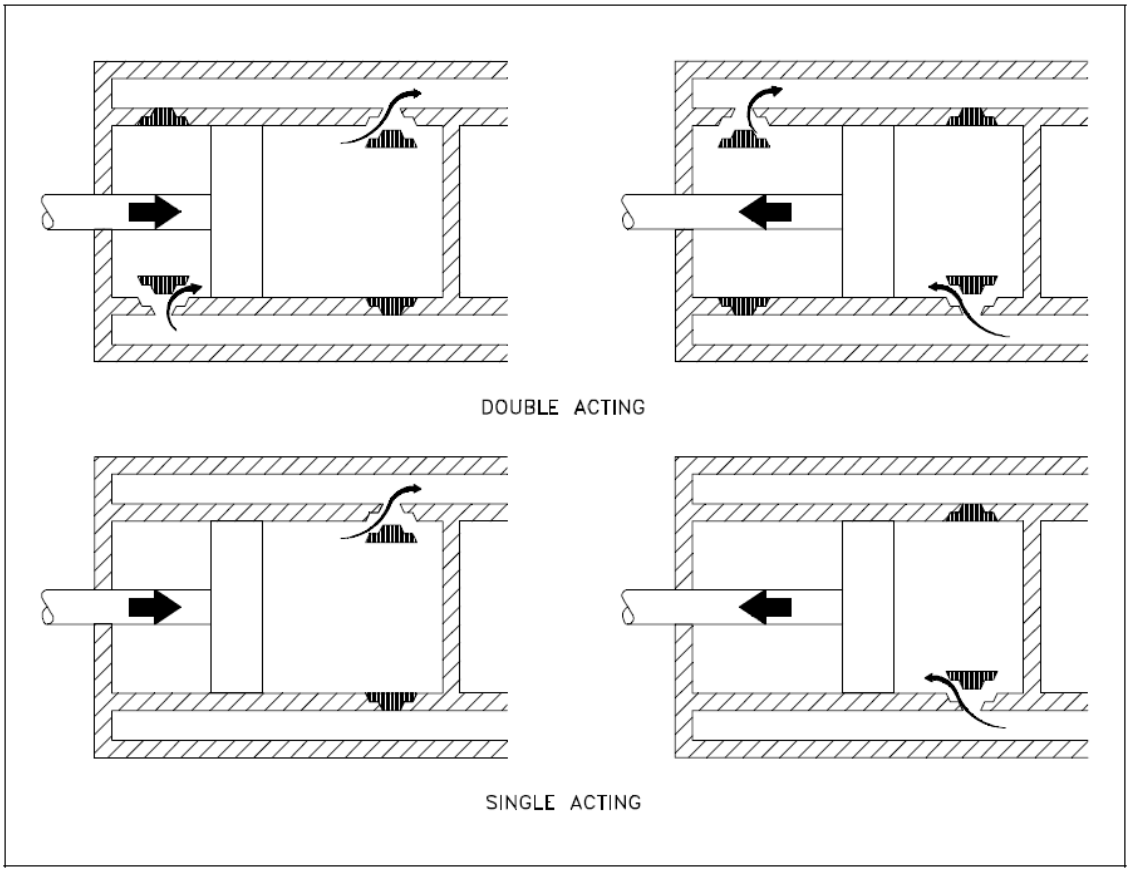

Figure 7: Positive Displacement Pump (Elie Tawil, 1993)

A PD pump has various types. Figure 7 shows two types which are the single action and double action. It could be seen that a check valve lets a set volume in and it displaced out the other valve. The double action has double check valves which allow it to have a constant discharge without pulsation of the fluid.

4.3.4 Microcontroller

A microcontroller consists of components working in unison to receive a command and through programming it will perform an action. Figure 8 shows the general layout of a microcontroller.

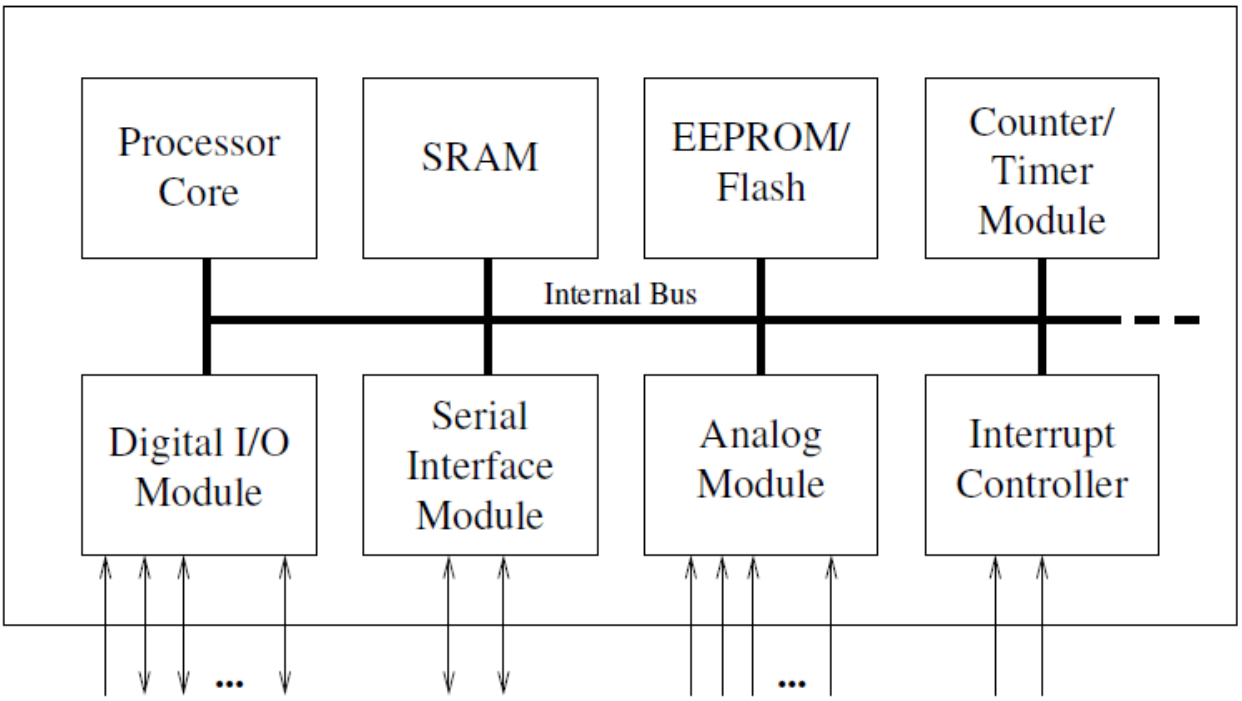

Figure 8: Basic Layout of a Microcontroller (Gunther Gridling, 2007)

The microcontroller will allow for the measurement of values which would be the input and according to the programming it will perform an operation. Microcontrollers can controller electric motors, they have the ability to control various external components without the need of a hard wire circuit. The versatility provided by microcontrollers is exceptional as any change can be performed through the programming intead of solder and wires. Also, their compactness allows their use in a wide variety of application in the field such as household appliance, automotive, aerospace and mostly any electronic that could be thought off will be using a microcontroller (Gunther Gridling, 2007).

4.3.5 Motors

The electric motor has been around for ages, one of the oldest types of electrical motor is the Barlow Wheel made by Peter Barlow in 1822 (See Figure 9).

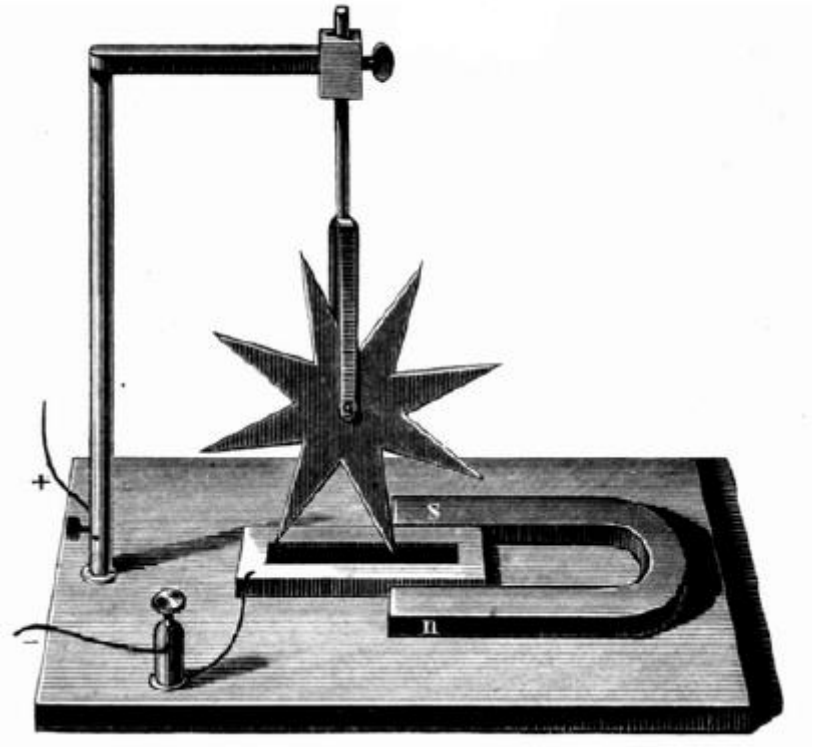

Figure 9: Barlow Wheel (Ucke, 2004)

The Barlow wheel is considered a novelty toy since it has low power and no practical application, but it shows the principle of an electric motor as it shows a continuously flowing current and continuous motion. The electric motor performs the energy conversion of electrical energy to mechanical energy. The electric motor has many different types of motor such as DC and AC current which according to each current the motors are further broken down to their types, such as a shunt motor, stepper motor, brushless motor, etc. The selection of a motor will be due to our design intent and the parameters required according to the performed calculations.

4.3.6 Thermo-couple

A thermocouple is a very simple method to attain a temperature reading using a microcontroller as the data logger. The principle of a thermocouple is rather simple, two conductors are connected in a close loop to a material, no since the material is different an electric potential is created in the closed loop. This referred to as the thermal electromotive force (Zhang, 2010). Figure 11 shows the thermal effect principle as the change in temperature could

be observed. By attaining the voltage difference of the thermocouple with the microcontroller the temperature could easily be found by converting the equivalent voltage to temperature.

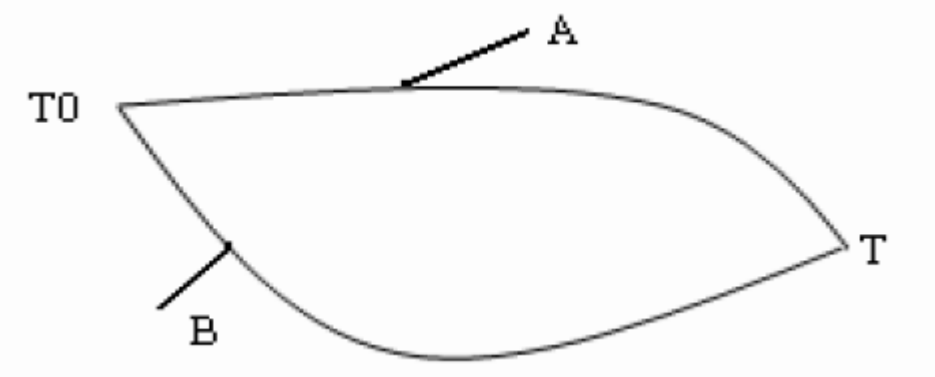

Figure 10: Thermoelectric Effect Principle (Zhang, 2010)

5. Project Objectives

The main objective of this project was to design, manufacture, and test a reliable test bench. This test bench task was to measure the MCE of materials. The device was designed in a manner which allows the operator to easily, and safely, replace the material specimen to be tested. A simple, yet efficient, design allows for the device to run cyclically with little need for maintenance. User, Repair, and maintenance manuals for the device will be provided. A display allows for the user to easily set boundary conditions for the system as desired, and doubles as a place to look for all dynamic signals coming from the various sensors within the system.

Overall, a test bench which is easy to use and reliable is what has been designed. A quick run-through of the user manual will allow anyone with slight knowledge of machinery to successfully use the device and acquire the data necessary. The option to export data to an excel spreadsheet has also been implemented in order to provide the user with a complete end user experience.

6. Designs

This project was a new experience for the team E-Mech. Various design alternatives were necessary as more research was performed, and constraints and budgets were changed. The first three designs were individually done by the team members in order to allow for each multiple design options without any bias opinions. This allowed for a wide spectrum of designs to choose from.

6.1 Design #1

The first design (See Figure 11) is a linear design where the material will reciprocate from one heat exchanger to the other. The design is composed of thermal electric plates on one extremity and a copper heat exchanger in the other with water as coolant. Figure 12 shows the location of the magnets and the thermo electric plates below for the heat rejection stage of the material.

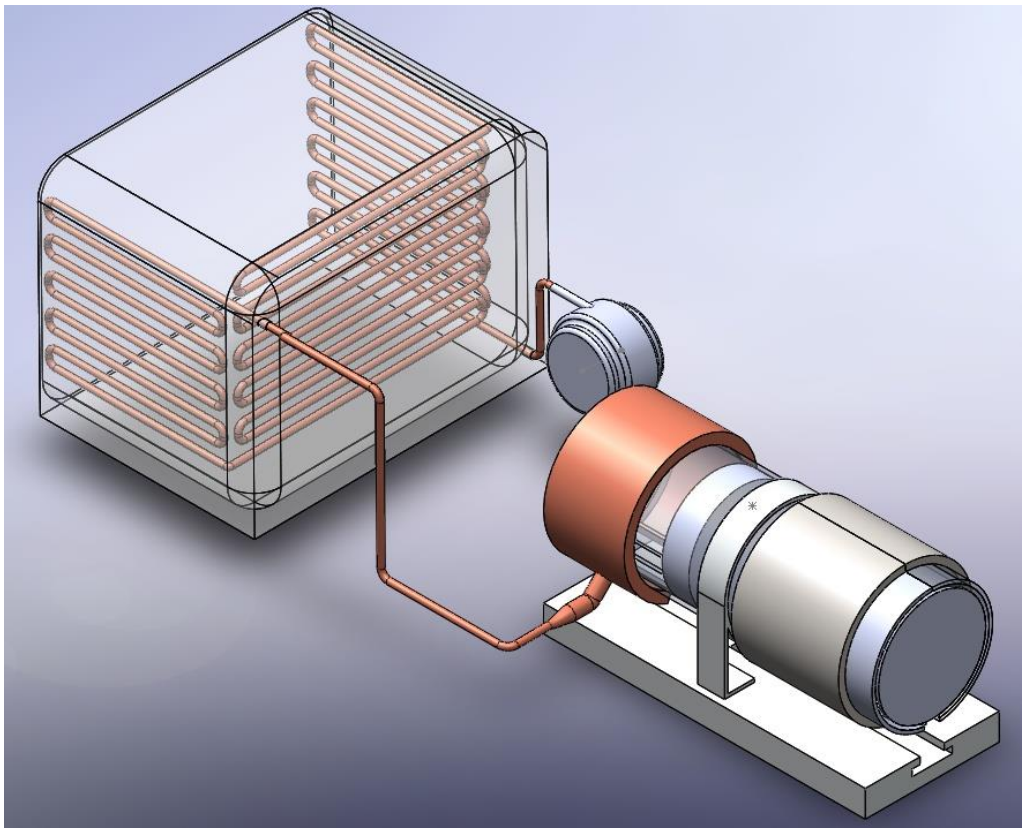

Figure 11: Design #1 (Linear-Reciprocating)

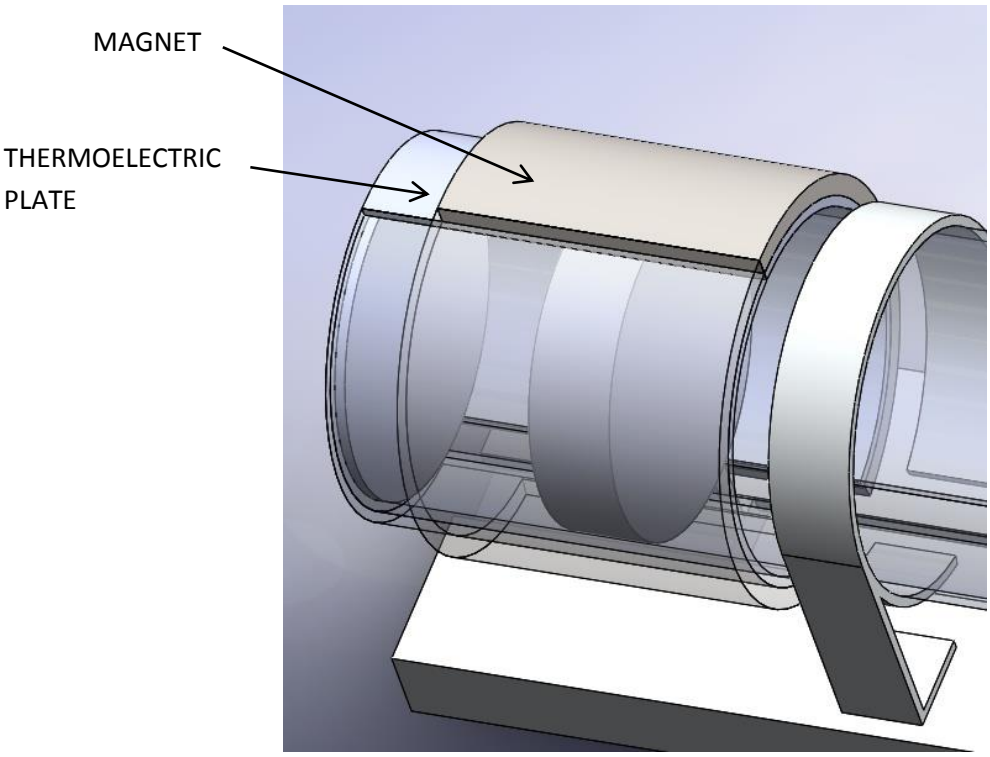

Figure 12: Magnets and Thermoelectric Plates

The advantage of this design is that the linear motion would allow the material to stay longer periods of time in contact with each heat exchanger. A higher heat removal is beneficial as it would provide a higher ΔT to use in the heat absorption stage. However, this design does not come without its disadvantages, the main one being the puck has a small contact surface area, so although contact time is increased the smaller surface area counter acts the benefits. Also, the reciprocating motion would have the material move from one heat exchanger to the other, which means that at any given time one of the heat exchangers would be consuming power without any heat transfer happening due to the material current position.

6.2 Design #2

Design #2 (Figure 13) uses circular motion where the material is spun through various chambers. The benefit of this design is that a circular motion allows for a larger surface area of contact with the heat exchanger in comparison to design 1. Also, the motion mechanism would decrease cost as all that it is required is an electric motor attached to an arm.

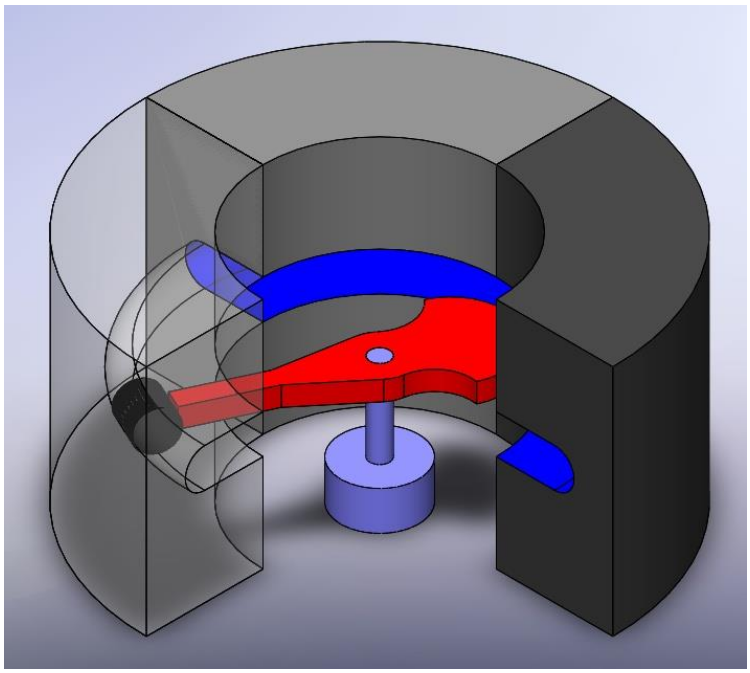

Figure 13: Design #2 (Rotary)

The enclosing chambers (Figure 14) insulate the system making a semi hermetically sealed system giving more accurate results towards the ΔT of the material. Consequently, this design suffers from the same issue as design one where, at any given time, one of the heat exchangers is not doing any heat transfer. This design would be very labor intensive due to the complex geometry of the curved chamber. This would imply high cost of manufacturing theses chambers via mold.

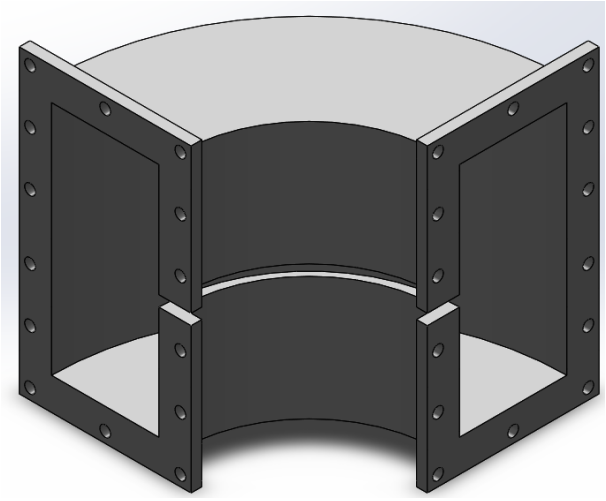

Figure 14: Enclosing Chamber

6.3 Design #3

An additional rotational approach was rendered using chambers similar to design 2 but involved closely encasing the material shape. Design 3 (Figure 15) uses the circular chamber approach that envelopes a spherical test specimen at a small clearance. This iteration provides a cost benefit due to readily available tubes. Rotational motion will allow for a simple mounting mechanism as well as provide a high surface area for convective heat transfer.

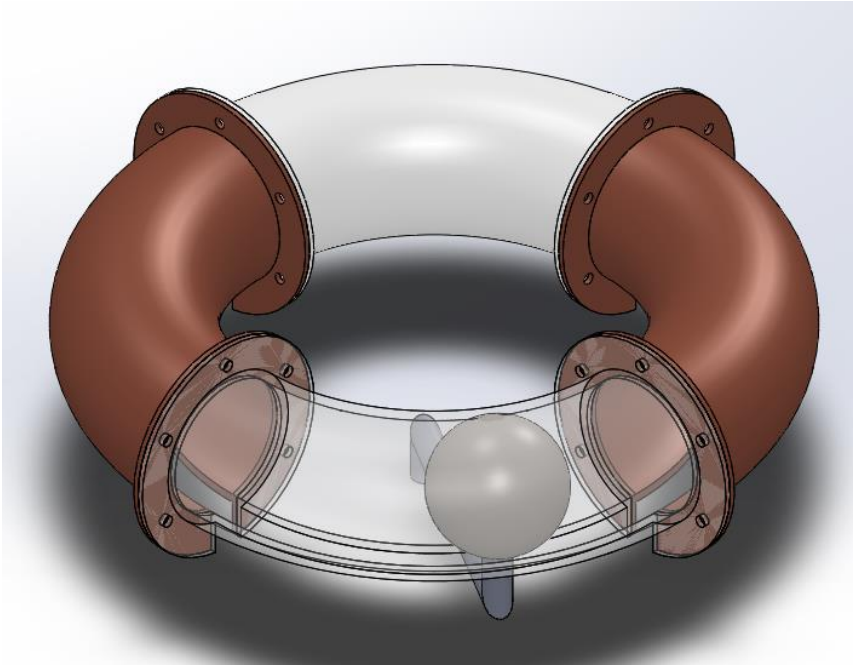

Figure 15: Design #3 (Rotary)

The disadvantage, however, of design 2 is the complexity of molding the material specimen into a sphere, surface stress created when magnetizing the spherical test piece, and small surface areas closely in contact with the heat exchangers.

6.4 Design #4

The final design (Figure 16) was not any of the previous mentioned designs, but rather a design where the advantages of all three initial designs were implemented and the disadvantages minimized.

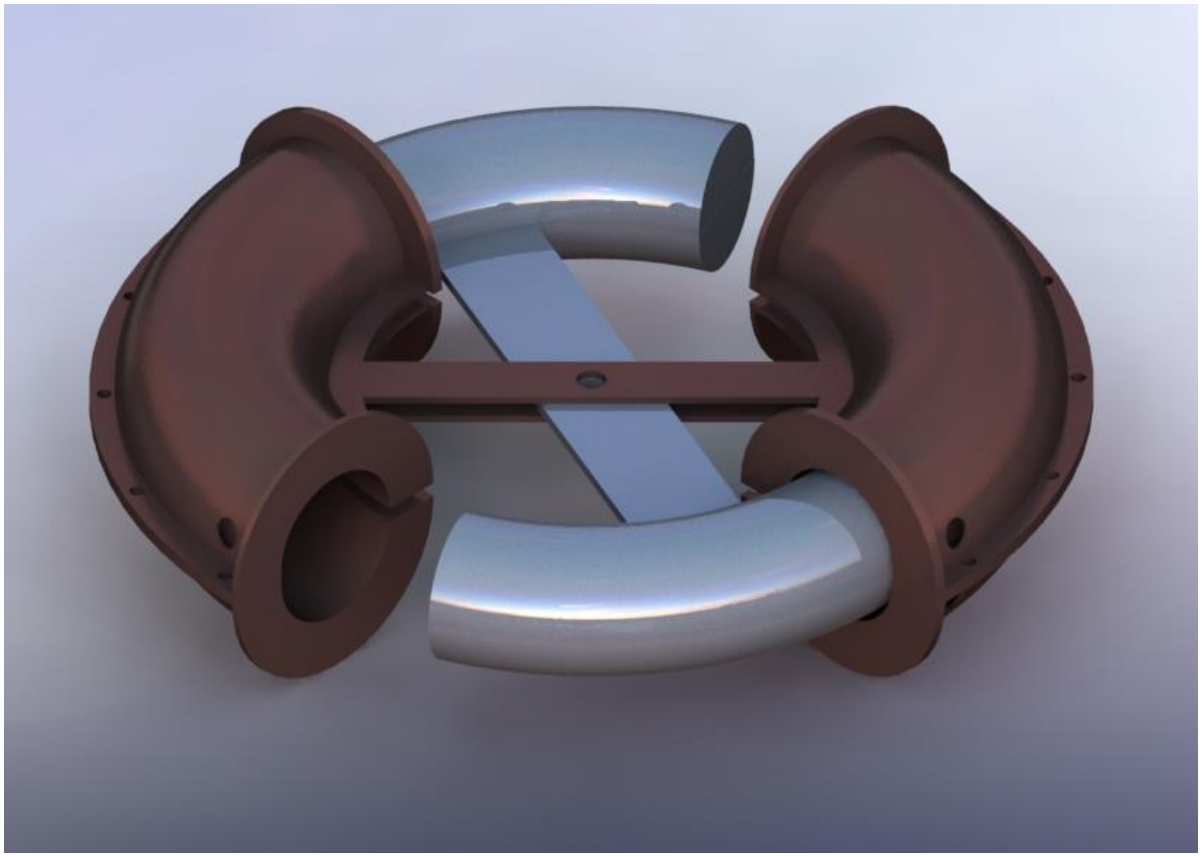

Figure 16: Design #4 (Rotary)

The advantages design 4 introduced were substantially greater than all other previous designs beginning with the movement mechanism. As seen in figure 16, a circular approach was taken due to the simplicity of the mechanism to put the material in motion. Furthermore, using a tubular design allowed for ease of manufacturability since copper pipes are commercially available. Figure 18 shows an improved material shape as this would be easy to cast compared to a spherical shape. Also, high surface area for heat transfer and the double material opposing each other would make both heat exchangers transfer heat at any given time.

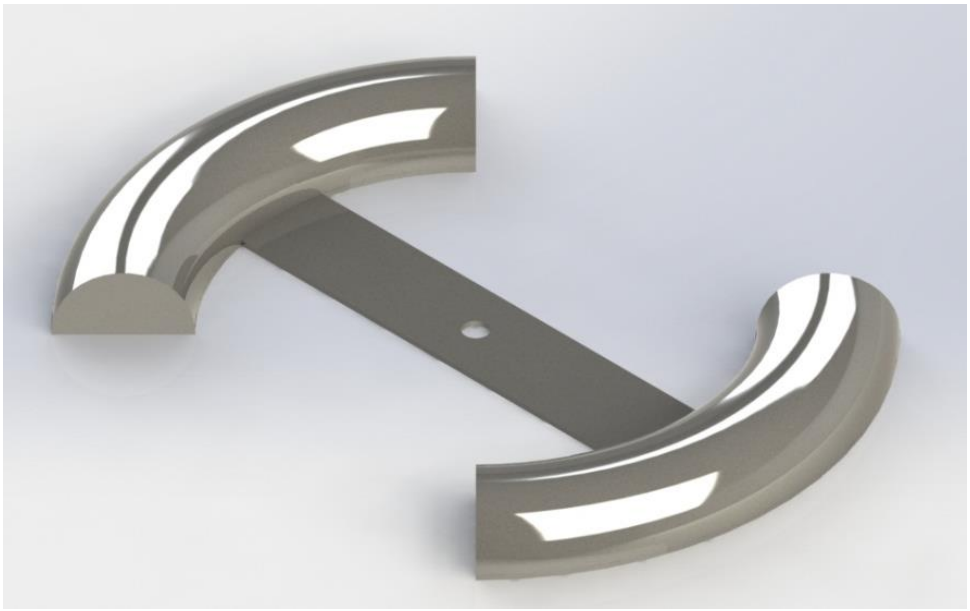

Figure 17: Material Specimen

The design uses Neodymium magnets (figure 19) of .125 in diameter and .063 in thick. The inside of the chambers will be lined with the magnets for the magnetization stage. These magnets produce a flux density in range of 1.25 to 1.28 Tesla which is a decent flux density for our purpose (Magcraft, 2013).

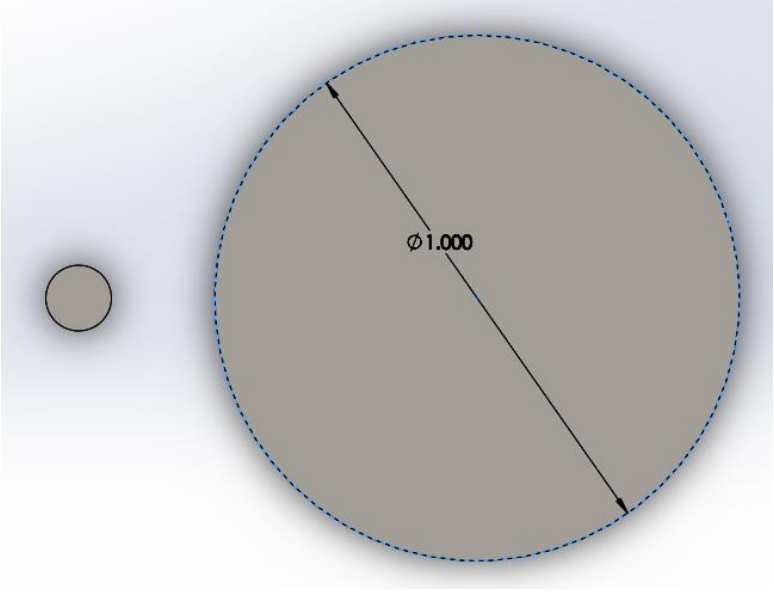

Figure 18: Size comparison of Magnet to 1" Circle

The heat exchanger for this design will be plate heat exchangers as mentioned previously they have a very high thermal performance. Our system is a low pressure, high flow application which would dictate the why a plate heat exchanger (Figure 19) was chosen.

Figure 19: Plate Heat Exchanger (Bartlett, 1996)

6.5 Final Design

Studying the pros and cons of the four preliminary designs, the final design produced the most efficient aspects towards the goal of the project. The design's mechanism (Figure 20) involves rotational motion similar to designs 2 through 4. Different from the concept designs, however, is the rotational motion of the magnets about the test piece instead of the test piece through the magnetic field. This simplifies the heat transfer between the heat exchanger and the test material. The stationed material provides a more stable and uniform heat transfer versus acquiring a uniform heat transfer between a stationary exchanger and revolving material.

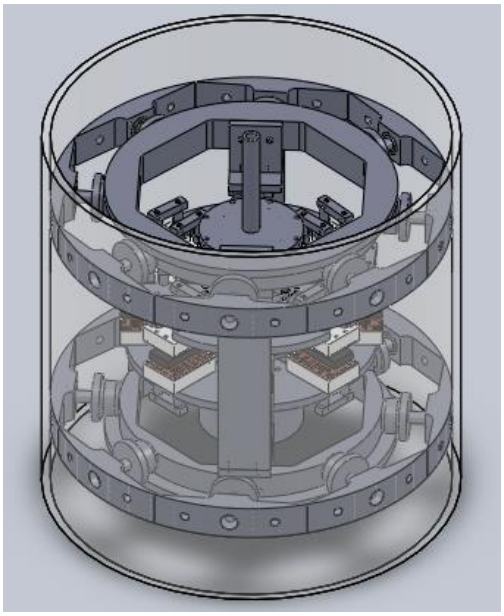

Figure 20: Final Design Mechanism

As opposed to a single or twice the number of test pieces, the final design exhibits a total of eight rectangular testing samples fixed in a circular pattern about an axis. The magnets are held in place with the use of brackets and set screws (Figure 21). In this design, two rows of small magnets, placed in a curved fashion, mirrored equally about the center are aligned along two curvatures enclosing two test pieces at a time (Figure 22). This would allow a uniform magnetization in only one direction of the material on opposite ends of the machine.

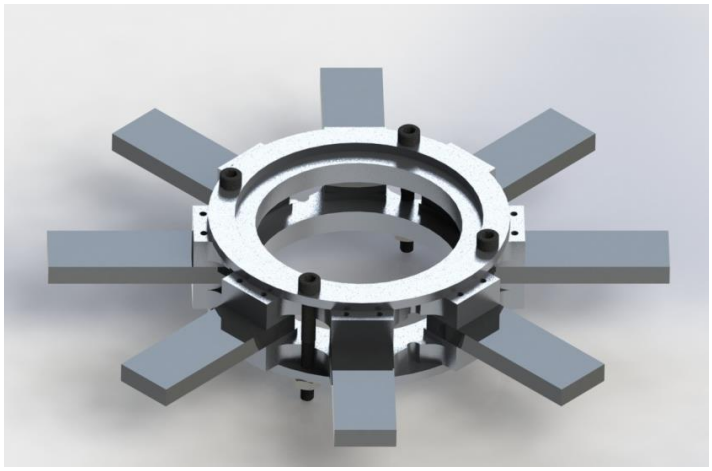

Figure 21: Material Wheel

Two heat exchangers are suspended above and below for every test piece on the material wheel. Upon engagement from the cam system, a heat exchanger may either drop or rise up to and make contact with a test piece resulting in a uniform heat exchange involving conduction and convective mediums.

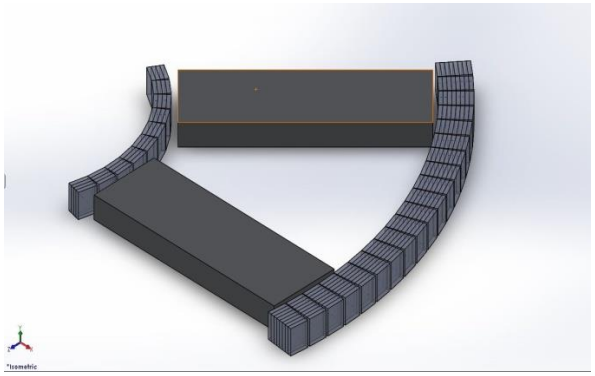

Figure 22: Magnet Placement

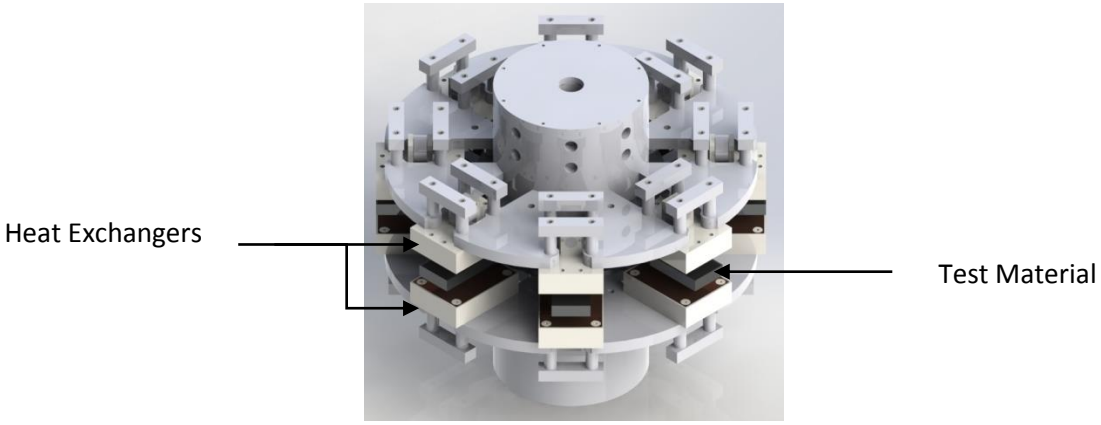

Figure 23: Main Wheel Assembly

7. Selection Analysis

7.1 Material Selection

The material selection for this project is critical as the heat rejection and heat absorption are the two most critical stages of the process. The material must have a high thermal conductivity to allow the most heat transfer as possible. Table 2 shows various materials and their thermal properties and it could be seen that the thermal conductivity of copper is substantially greater than the other materials in the table. Although this table does not provide all the possible materials it does show the materials currently used for micro processing which carries out the similar heat transfer scenarios for this project. The thermal conductivity "K" is the most critical property of the material during the selection process. This material must also carry long life and must be resistant to relative wear and damage throughout the machine's operative life.

Table 2: Thermal Properties of Materials

Item	Material	Characteristic Dimensions (mm)	Characteristic Thickness (mm)	Thermal Conductivity (W/m-K)
MOSFET (IXFD21N50)	Silicon	8.84 x 7.19	0.425	118
DBC Ceramic Substrate	Alumina (Al_2O_3)	28.45 x 27.32	0.635	26
DBC Base	Copper	28.45 x 27.32	0.3	395
DBC Traces	Copper	N/A	0.3	395
Hybrid Gate Driver	Alumina (Al_2O_3)	21.08 x 8.51	0.635	26
Ceramic Frame	Alumina (Al_2O_3)	27.32 x 25.4	0.625	26
Dielectric Layer	Polyimide	N/A	0.125	0.3
Epoxy Interface	Epoxy	N/A	0.3	1.4
Gap Filler	Silicone Gel	N/A	0.254	0.2
Chip Attached	Solder	N/A	0.127-0.475	51

7.2 Heat Exchanger

Selection of a heat exchanger requires analysis on the application of which it is to be used. The final design requires a high thermal performance and low pressure heat exchanger which would make a plate heat exchange ideal. Due to the small dimensions of the test material, however, this project

demands the manufacturing of custom designed heat exchanging units. Nevertheless, the thermodynamic properties and fluid mechanics for heat exchangers remain unchanged.

The fluid fundamentals for heat transfer are largely due to the fluids characteristics such as the density, specific heat, thermal conductivity and viscosity. One of the major dependencies is fluid flow as inside a heat exchanger the flow could be laminar or turbulent. A laminar flow solely uses the thermal conductivity of the fluid as opposed to turbulent flow which produces a convective and thus larger heat transfer (Bartlett, 1996). The governing equation for the behavior of a fluid flow is Reynolds number:

$$Re = \frac{\rho * v * D}{\mu}$$

Where the v is the fluid velocity, D is the tube diameter and u is the dynamic viscosity of the fluid. A Reynolds number higher than 4000 is considered turbulent flow. Although turbulent flow provides higher heat transfer it will greatly affect the pressure drop through the heat exchanger requiring more pumping power. The heat exchanger is governed by the balance equation:

$$\dot{Q} = \dot{m} * C_p(T_{out} - T_{in})$$

The balance equation must be balance meaning that the heat transfer from the hotter fluid to the colder fluid must be equal to each other. The mass flow rate $\dot{m}$ is what would allow for a more effective convective heat transfer as long as the behavior of the fluid remains turbulent (Bartlett, 1996). Turbulence would then result in higher volume flow rate values for the given diameter which would require a series of costly pumps. Therefore, a balance between cost of a pump unit and design of a heat exchanging component is crucial to meet specific project requirements such as budget versus minimum angular velocity of the central shaft which powers the assembly.

The effectiveness of the heat exchanger or better known as the efficiency for the heat exchanger is given by:

$$\varepsilon = \frac{(\dot{m} * C_p)_{hot} * (T_{in} - T_{out})_{hot}}{(\dot{m} * C_p)_{min} * (T_{in\,hot} - T_{in\,cold})}$$

The denominator of the equation is the maximum heat transfer rate of the heat exchanger (Bartlett, 1996). Figure 20 shows how the temperature changes according to the length of the exchanger and the effectiveness.

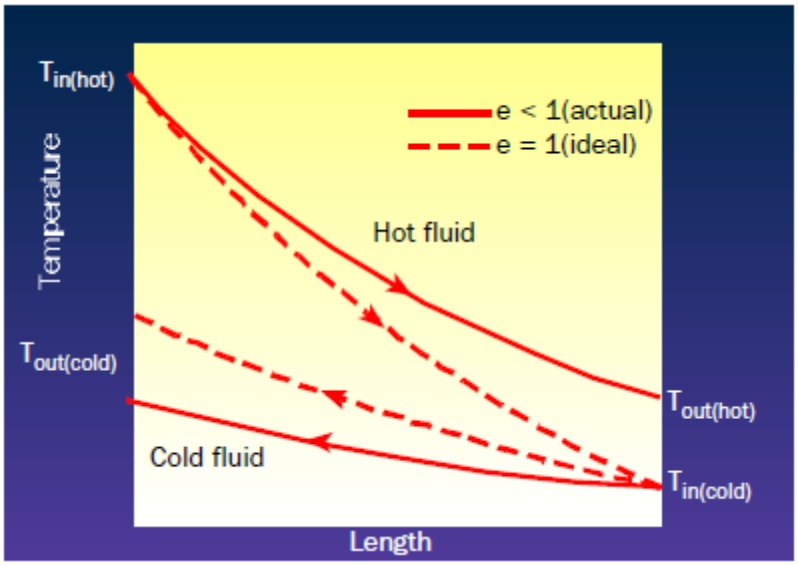

Figure 24: Stream Temperature through a Heat Exchanger (Bartlett, 1996)

The thermal performance of the heat exchanger is calculated by:

$$\dot{Q} = U * A * \frac{(T_{in\ hot} - T_{out\ cold}) + (T_{out\ hot} - T_{in\ cold})}{2}$$

where U is the heat transfer coefficient and the heat exchanger area (Bartlett, 1996). The heat exchange from the material to the exchanger will happen through convection and conduction as the magnets spins about the material. The convection equation is:

$$\dot{Q} = h(T_{hot} - T_{cold})$$

Determining the total transfer to a fluid the thermal resistance equations are used to evaluate values such as heat transfer rate and heat flux.

7.3 Pump

The method in choosing a pump calls for preliminary assumptions such as knowledge of the volumetric flow rate, working fluid, and the ambient pressure the MCR system will be working under. Given these parameters the pump, with respect to horsepower, is governed by equation:

$$HP_{min} = \frac{\frac{\text{GPM} * \text{PSI}}{1710}}{\eta}$$

This equation provides the engineer with power from which a particular pump may be chosen from any catalog with respect to English units. GPM is given as gallons per meter and PSI is a value of pressure given as pounds per square inch. Given the small dimensions of the final design, the pump is to be manufactured to meet specific sizing and operation of the thermodynamic process involved for the project.

8. Major Components

The design and build of the MCE testing machine features high influencing components crucial to the functionality of the refrigeration cycle. In other words, without the full contribution of certain elements in the design, the system will not function as expected. The components that are termed as “major” are:

- Heat Exchangers
- Magnets
- Electronics
- Pump

8.1 Heat Exchangers

8.1.1 Properties, Assumptions, & Estimates

The determining factors for designing the most effective heat exchanger is the total head produced by the system, the volume flow rate desired for the fluid, and the conductive surface from which the energy transfer will take place. Specific assumptions were taken into account in order to grasp a theoretical basis for the operation of the heat exchange. Existing designs of heat exchanging units were also surveyed in order to determine an optimum layout for the unit. Firstly, based on analysis from material selection and budget limits for the project, water will be the convective medium of choice and a thin copper plate will be utilized as the conductive medium for the transfer of the heat energy. Copper holds one of the largest conduction coefficients for commercial grade metals providing large transfers of heat between bodies of material. Water is the most frequently used and easy accessible material available for small heat recovery applications such as the MCR test bench.

Fluid analysis reveals evidence that turbulent flow would provide the largest convection factor for liquid versus solid surface contacts. A value of 4,000 Re was used to illustrate a rough calculation for the behavior of the flow, in this case turbulent, in order analyze the average velocity of water during the heat exchange. Using the equation for Reynolds Number and basic kinematic equations, the velocity of the fluid at the impeller into the channel before the heat

exchanger is estimated to be 0.38 m/s. From the channel into the heat exchanger, due to the abrupt change in diameter, the velocity changes to 0.75 m/s because of the decrease in diametric size. This would mean that the volume flow rate that the heat exchanger would see has a value of 4.21243E-5 m^3/s.

Performing a steady state analysis of the heat transfer process, the basic outline of the transfer was illustrated by figure 25. Specifically, the diagram depicts a steady state 1-Dimensional heat transfer through the thickness of the copper plate into the test material and into ambient conditions of air and water. Here, “k” is used to describe conduction coefficient; “t” shows thickness of the adjacent materials; subscripts “c” and “m” describe the copper and material components respectively; “q” represents the heat transfer rate into or out of their respective sources. The illustration above assumes an energy source is starting at the centroid of the test piece resulting from the magnetic influence of the magnets. This heat source, through conductive means, is branched either into ambient air or, most preferably, fluid flow.

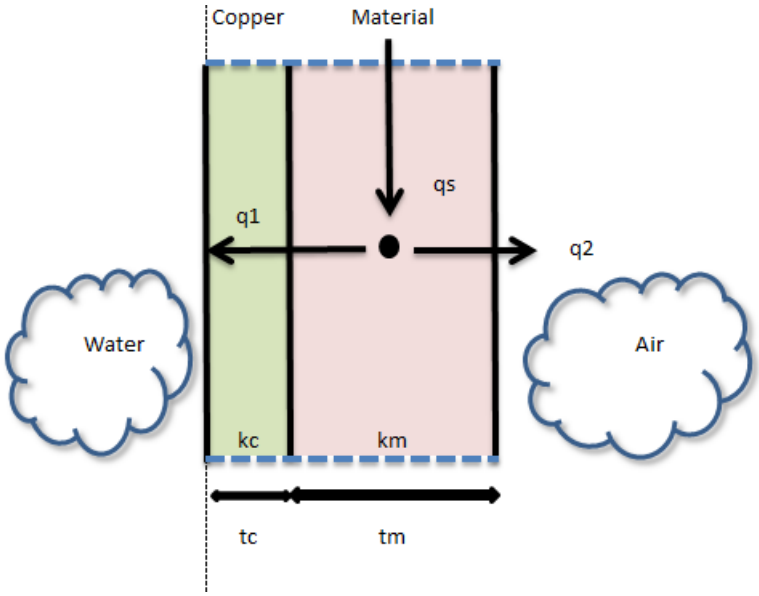

Figure 25: 1D heat transfer diagram

Using thermal properties for each medium, basic resistive heat transfer methods, Newton's law of cooling, as well as assuming a temperature rise of 298K to 303K, table 3 was constructed:

Table 3: Thermal parameters

Water		Copper		Air		Material	
T (K)	298	K (W/m2K)	401	T (K)	298	t (m)	0.00635
h (W/m2K)	13	t (m)	0.0006096	h (W/m2K)	10	A (m^2)	0.000968
		A (m^2)	0.001261933			T(K)	303

From table 3 the following results are estimated:

Table 4: Heat transfer results

Material	Iron
k (W/m2K)	80
R1	60.998761
R2	103.37455
q1	0.0819689
q2	0.0483678
H.Transfer (qs)	0.1303367

The heat source is theoretically calculated to have an average value of 0.13 watts assuming the test piece an iron-based composite. The values "R" represent the characteristic thermal resistance across the thickness of the conductive material.

Another consideration for designing this heat exchanger is the fluid volume that is readily available within a given amount of time. There exists a short time period where a single piece of material experiences magnetization. During this magnetization process, the exchangers are to make contact with the test pieces. Therefore, this time frame is inversely proportional to the angular frequency of the central shaft imposed by the motor. This time frame is responsible for the rate at which water will flow through the channel from inside their respective pump and into an exit of a ¼ inch diameter. The method for averaging this window of fluid flow requires assuming a series of impeller frequencies from maximum to minimum, and the total arc length

of travel the channel opening needs to accomplish from opening of the port hole to closing of the port hole.

Table 5 illustrates rough estimates different opening time periods at different frequencies imposed by the shaft on the impeller. This estimate was derived by measuring an arc length of 0.015707964 meters.

Table 5: Port hole duration calculation

Impeller		**Channel**			**time s**
impeller **rpm**	impeller **rad/s**	channel **rpm**	channel **rad/s**	channel velocity **m/s**	
300	31.41592654	107.1428571	11.21997376	0.336599213	0.046666669
162.54	17.021149	58.05	6.078981785	0.182369454	0.086132648
81.3	8.513716091	29.03571429	3.04061289	0.091218387	0.17220173

As a result, the following table involving fluid behavior may be tabulated by using equivalent channel diametric area and exit area using Bernoulli's balance equation.

Table 6: Volume flow rates and velocities

In the Channel		**After Port hole**	
Fluid Velocity m/s	Volume Flow m^3/s	Fluid Velocity m/s	Volume Flow m^3/s
0.699004365	3.91997E-05	1.3864072	7.77489E-05
0.378720565	2.12384E-05	0.751155421	4.21243E-05
0.189430183	1.06231E-05	0.375716351	2.10699E-05

Table 6 shows that the volume flow rate may allow for more fluid than what the channel may provide at a given time. This, however, does not assume any losses that may arise from abrupt geometries within the casing of the channel route or backflow at stagnation points.

8.1.2 Simulations

Forming a steady state analysis of the heat transfer problem and by using SolidWorks® simulations a transient thermal study was performed. Figure 26 represents the starting temperature plot at 0.25 seconds between the copper plate and the material block in thermal

contact. The material is assumed to hold a uniform constant surface temperature of 303K while the copper plate holds an ambient temperature of 298K. Figure 27 illustrates an equilibrium temperature at 1.25 seconds. Both copper and test piece share a similar temperature of 303K.

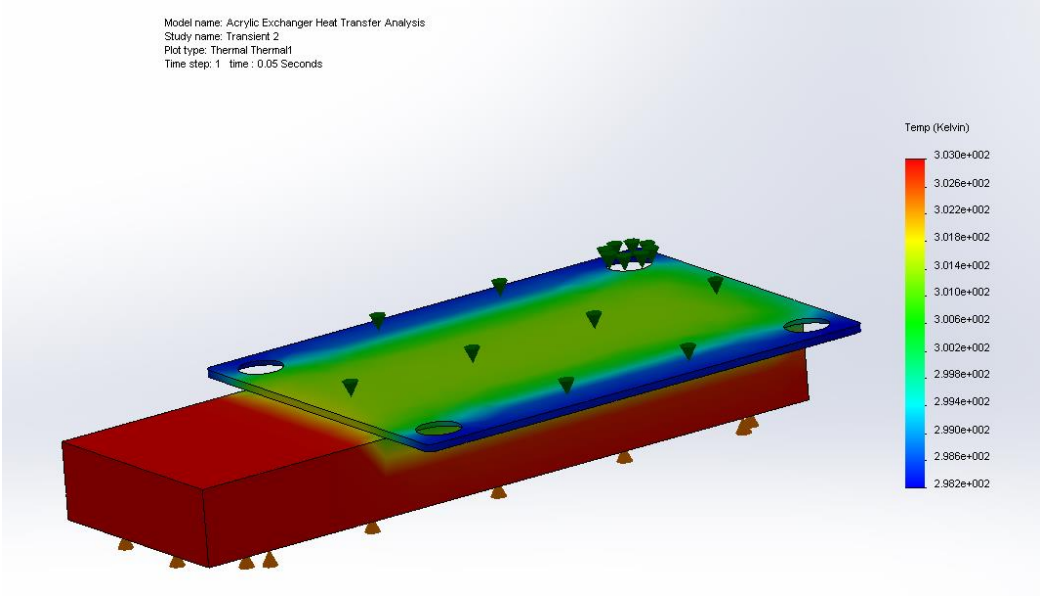

Figure 26: Transient heat transfer @ .25s

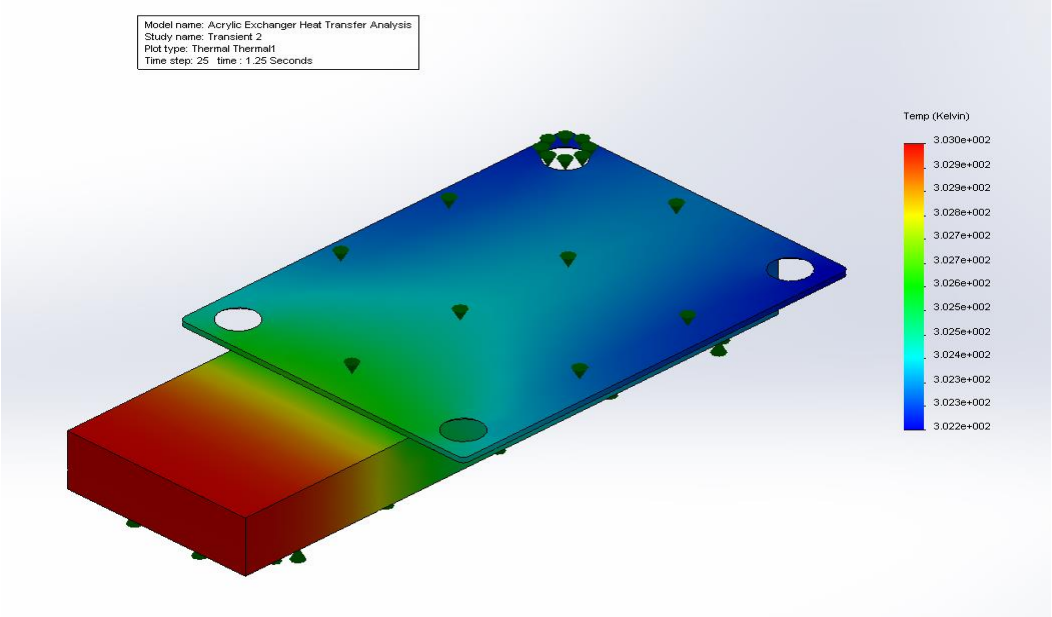

Figure 27: Transient heat transfer @ 1.25s

Overall, the simulations provides promising indication that the values obtained effectively correlate to the assumed parameters from any analysis that was conducted beforehand.

Judging by the estimates and assumptions previously estimated, the final design for the heat exchanger involves a hybrid style copper-plated shell and tube unit. The design of the heat exchanger that is to be implemented for the MCR test bench can be seen in figure 28.

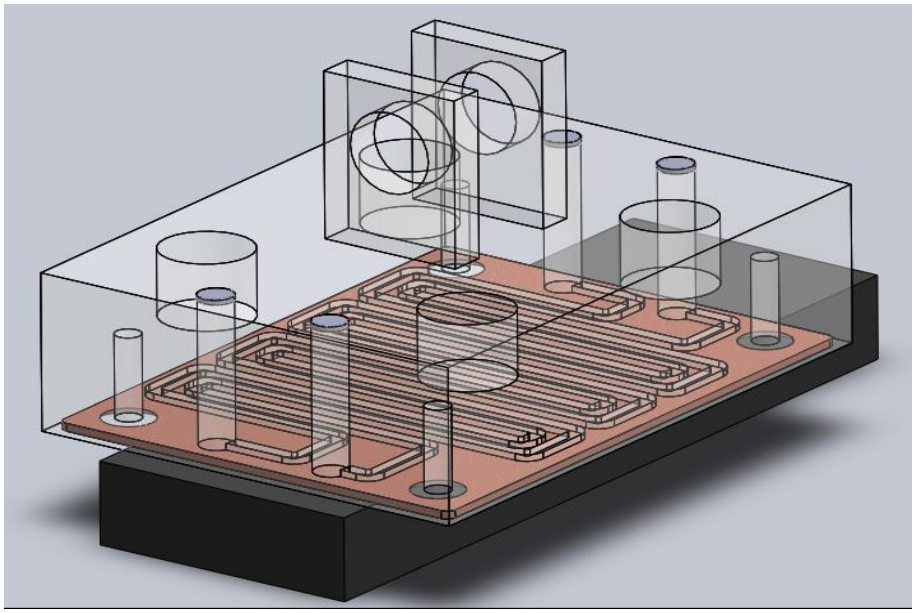

Figure 28: Final heat exchanger design

Ultimately, the casing for the heat exchanger will have machined contours in a linear pattern from one end to the other. This layout would provide maximum coverage of are where the convective medium may make contact with the copper surface. The casing consists of a pair of inlets and outlets assuming a flow for heat exchange and secondary flow for cooling of the copper plate. The casing is made out of low density polyethylene to reduce any heat losses within the system. In accordance to the tabulated values and analytic evaluations made, this heat exchanger is expected to produce the most effective transfer rate of heat energy.

8.2 Magnets

The focus of this project centralizes on the use of magnets. Magnets are what define the unique processes within the MCR cycle. Most Magnetocaloric Refrigeration systems contain magnets capable of changing the intensity of their magnetic field. However, for the current task of developing a testing apparatus that will periodically run for lengthy periods of time For this case, the use of permanent magnets will used. Neodymium magnets provide the highest flux density and maintain a constant magnetic field at all operational temperature making it the only candidate in magnetic material.

The initial designs of the system consisted of static magnetic flux sources and dynamic material specimens. Due to complications with the heat exchange process that would result from this design, keeping the magnetocaloric material static and rotating the magnets proved to be a more effective choice. The goal for magnetization is to achieve a magnetic flux density of 0.7 Tesla at the midway point of the magnet assembly (as per Dr. Benjamin Boesl). Several design iterations were performed with respect to the choice of magnets. The boundary conditions for this choice were the magnetic density requirements as well as geometric constraints of the apparatus' design. Figure 29 shows the dimensions of the magnetocaloric material which will be subject to testing. The material is fastened into the device at 45° increments. This is due to the fact the material goes through four phases during the cycle and the test bench will run two cycles per revolution. Dividing the 8 materials equidistantly yields 45°angles in between each specimen. The material and the assembly fastening it can be seen in Figure 30.

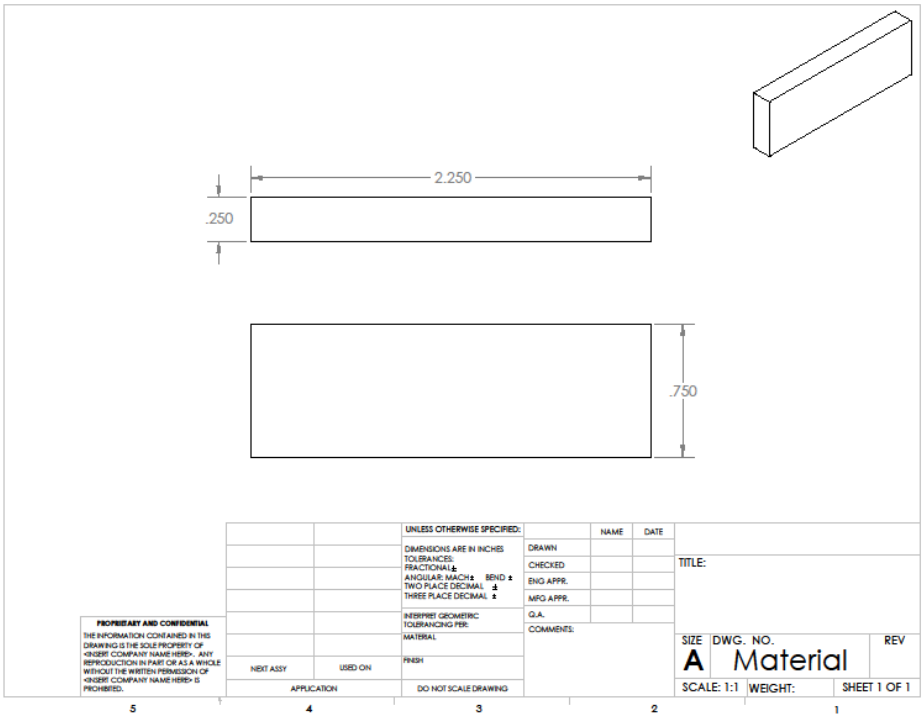

Figure 29: MagnetoCaloric Material

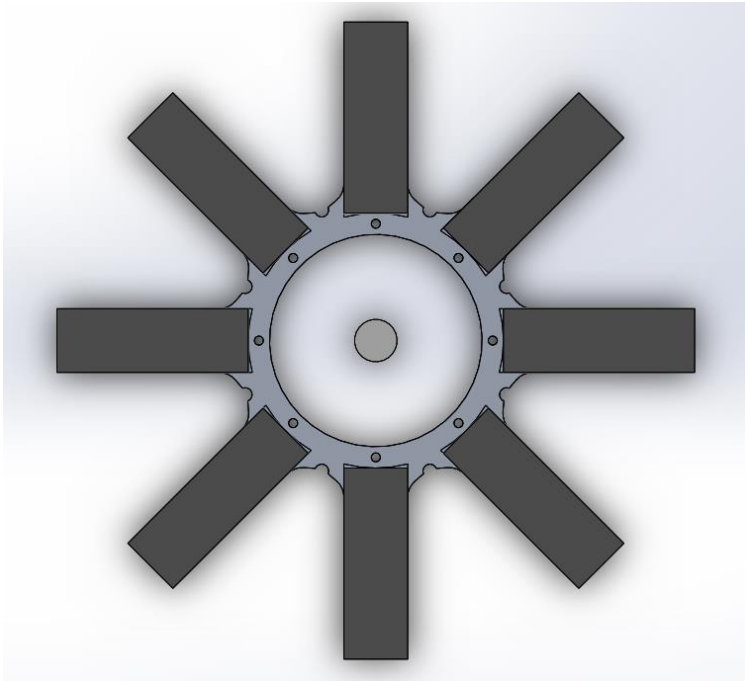

Figure 30: Material assembly

The first design iteration for the magnet selection/placement can be seen in Figure 31. The magnets selected were made of neodymium-iron-boron and rated at 1.27 Tesla. The red figures in the image represent the magnetocaloric material and the gray figure is the rare earth magnets.

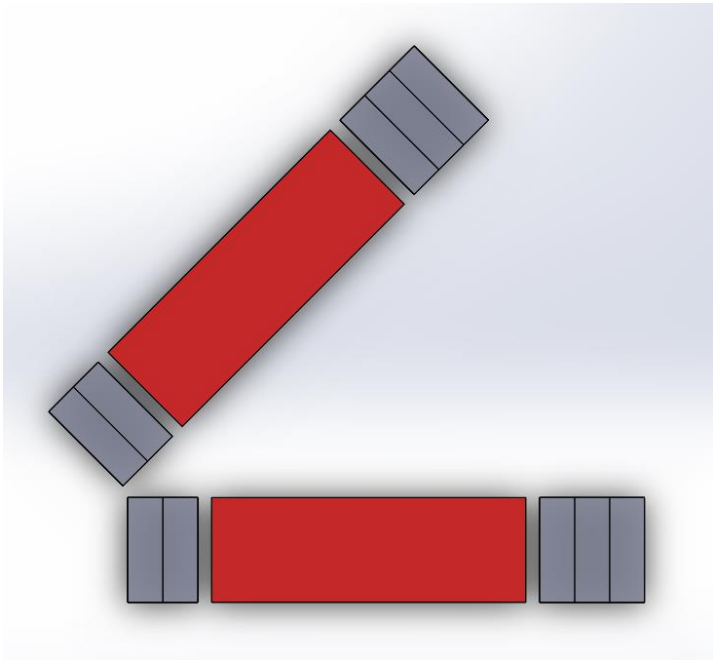

Figure 31: Magnet selection/Placement

Using SolidWorks© simulation software, supporting data for the alignment of the magnetic moments of the material was obtained. Also, values for the magnetic flux density throughout the material were obtained. Figure 32 shows the alignment of the magnetic moments through the material. The alignment is portrayed as blue vectors in the figure. Figure 33 shows a plot of the magnetic flux density versus position. The plot goes through both magnet assemblies, the air gap between the magnets and the material, and through the magnetocaloric material. An average magnetic flux density of 0.347 Tesla was obtained. The maximum magnetic flux density was found to be 0.358 Tesla.

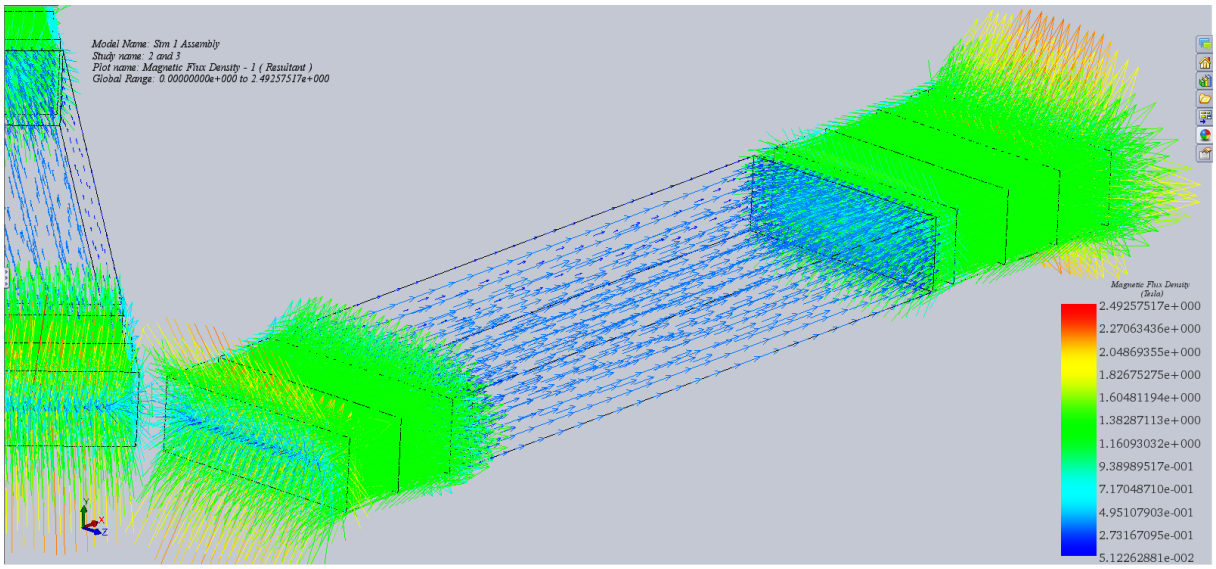

Figure 32: Moment Alignment

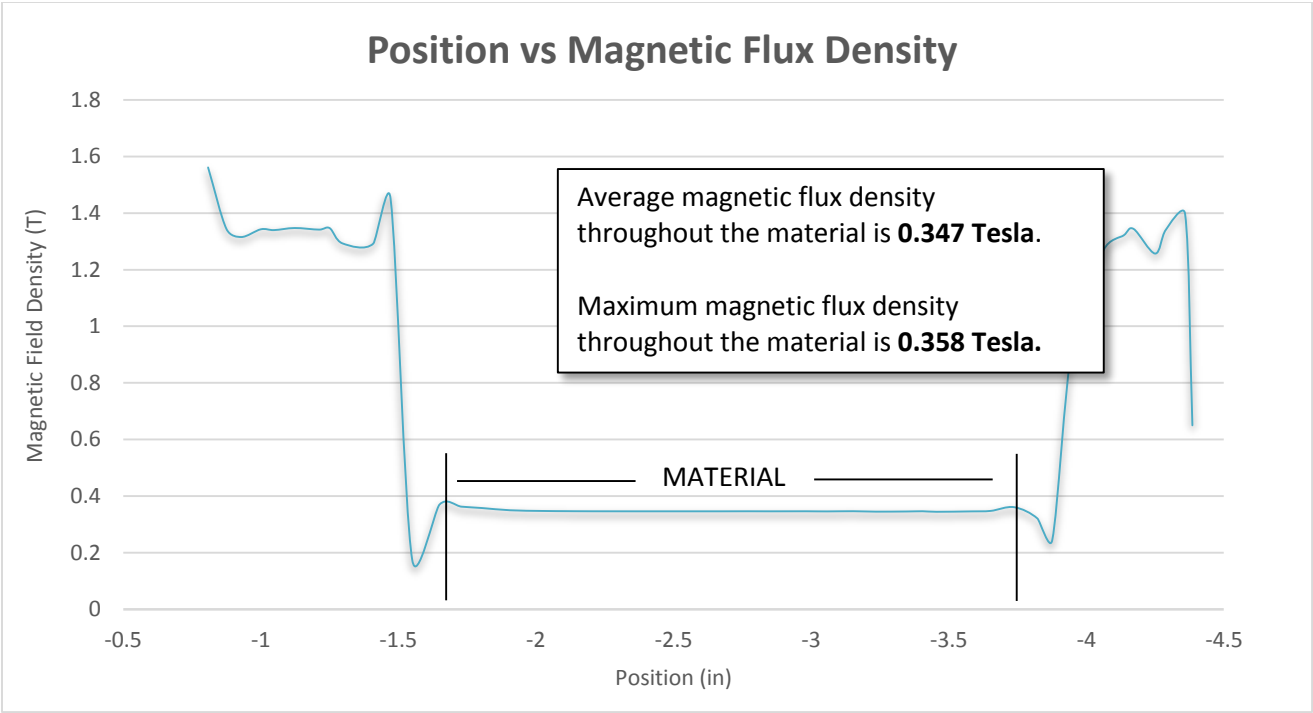

Figure 33: Magnetic flux density Vs. Position

The flaws with the first design iteration, aside from a low average magnetic flux density, were that the flux density would not remain constant as the magnets rotate. A top and isometric view of the geometry for the second design iteration can be seen in Figure 34.

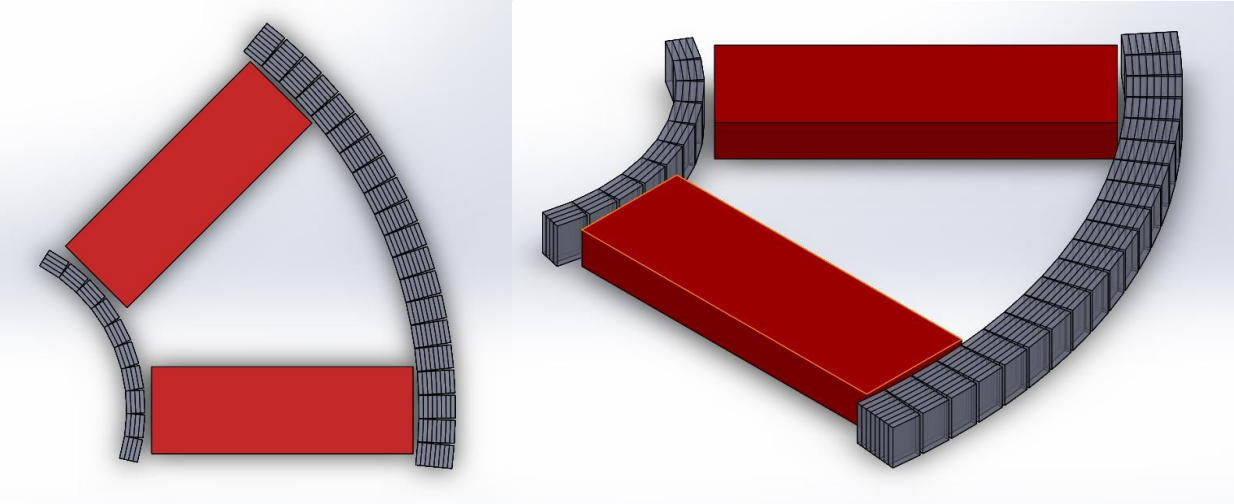

Figure 34: Top and isometric view of geometry design

Again, we have supporting evidence for the alignment of the magnetic moments of the material, as well as values for the magnetic flux density throughout. The alignment can be seen in Figure 35 and the plot of the magnetic flux density versus the position within the magnet can be seen in Figure 36.

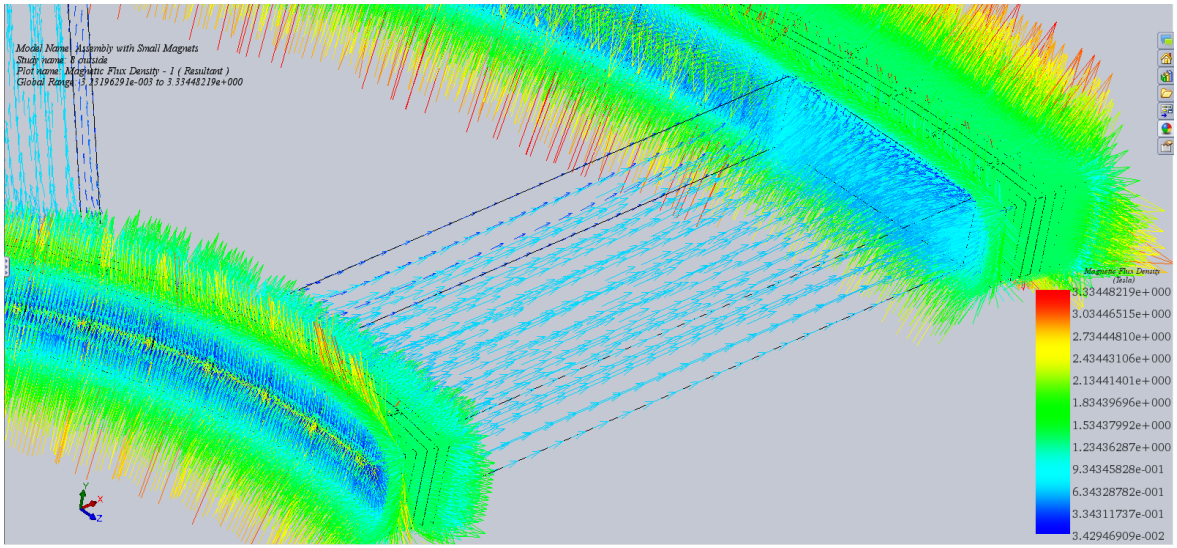

Figure 35: Magnetic pole alignment

The simulations for this second iteration yielded an average magnetic flux density of 0.639 Tesla and a maximum magnetic flux density of 0.659 Tesla. These values are much closer to our desired value of 0.7 Tesla throughout the material. The last simulation to be run was to see how the magnetic field and flux density within the magnetocaloric material would be affected due to the rotation of the magnets. In order to do this, the simulation was run with the magnets at a 5° offset so that the material could be half exposed to the magnets in the orthogonal direction. Figure 37 shows the material with the magnets at a 5° rotation. A slight misalignment was expected at the ends of the material where there was an offset between the magnetocaloric material and the magnets. Figure 38 shows this misalignment, however, it shows an overall alignment throughout the rest of the material. This misalignment at the ends of the material is inevitable.

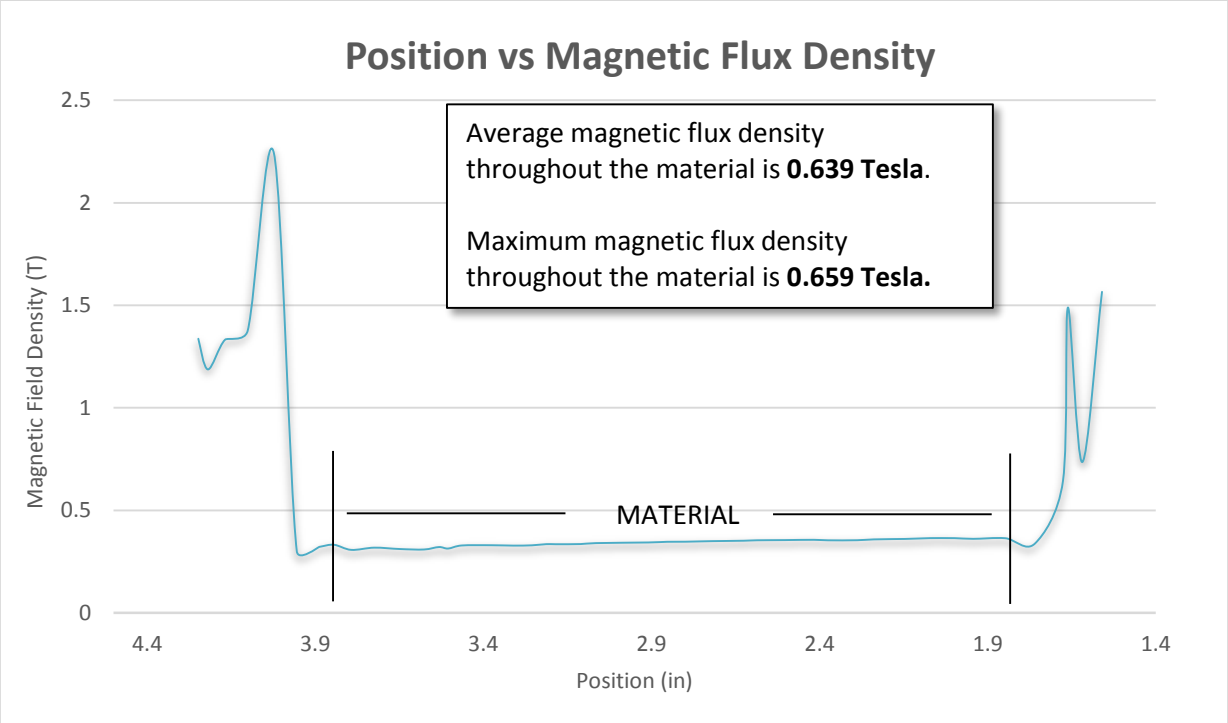

Figure 36: Position Vs. Flux Density (2)

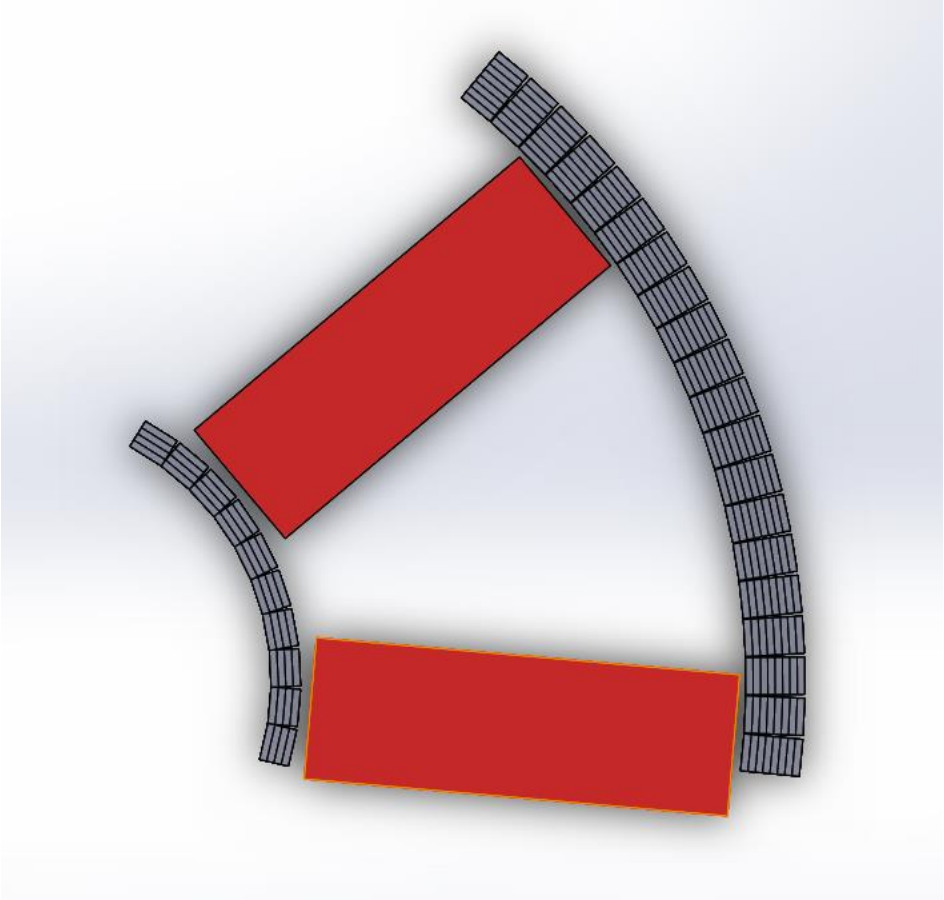

Figure 37: Magnets with 5 deg misalignment

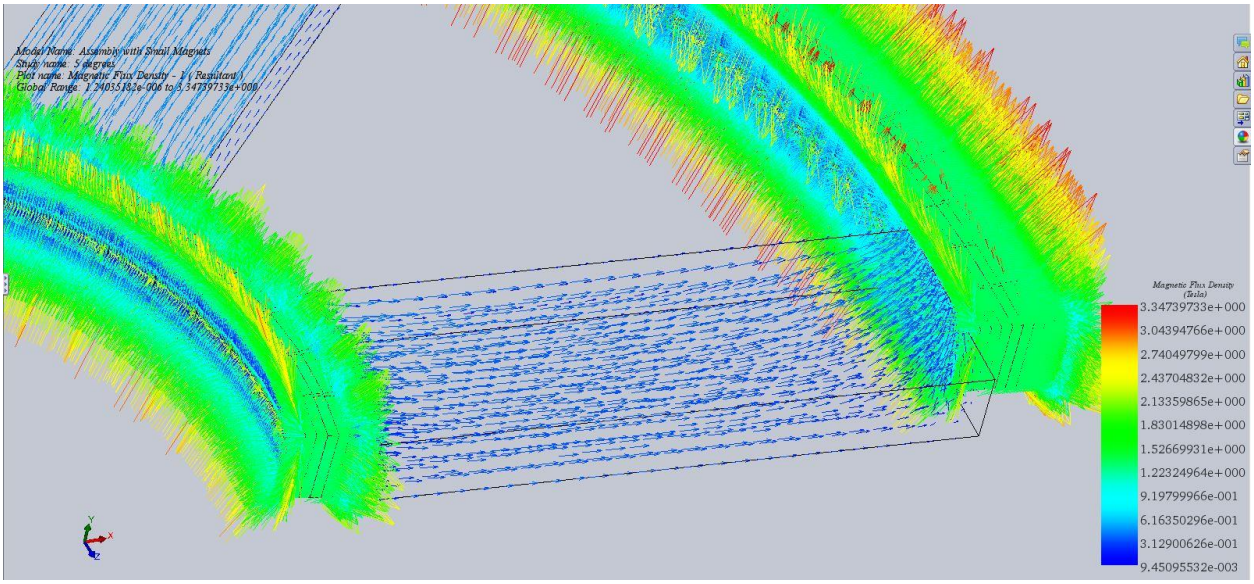

Figure 38: Magnetic poles with misalignment

An average magnetic flux density of 0.338 Tesla was obtained for the offset material specimen. The maximum magnetic flux density was found to be 0.364 Tesla. The plot of Magnetic flux density versus position within the material specimen can be seen in Figure 39. These simulations provided enough supporting data for selecting the second design iteration. A total of 200 neodymium-iron-boron magnets are necessary for this design.

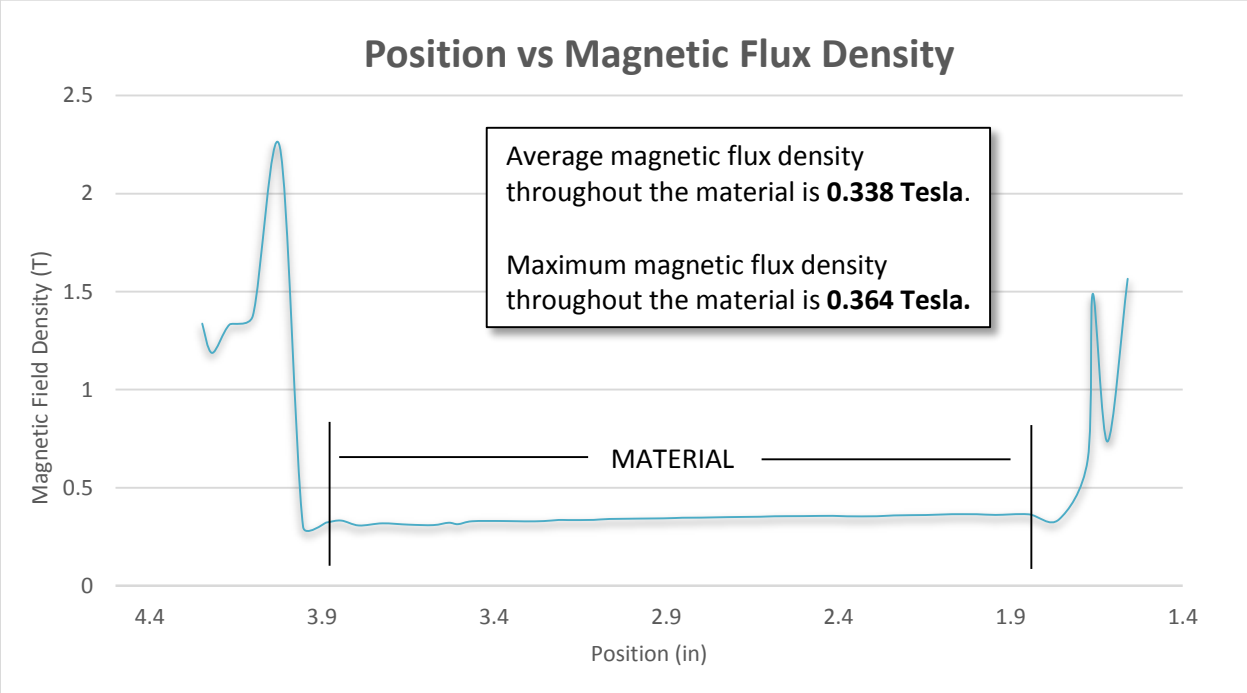

Figure 39: Position Vs. Flux density (3)

8.3 Electronics

Arduino packages will be used to display temperature on a screen as well as send signal in order to operate motorized components of the system. For this to work, circuits will have to be constructed after detailed planning of the circuit diagram. This portion of the prototype will be looked over and designed by an Electrical Engineer.

8.4 Pump

In order for any heat transfer to occur, a working fluid such as water needs to flow through a path that will enable it to extract heat from a source. This flow however is produced by a pump. The pump that is used in this design of MCF is a centrifugal pump. The testing apparatus, due to the applications and conditions, the centrifugal pump is preferred due to the system's low viscosity flow for water and the relatively low cost. Design of the pump is also dictated by the amount of fluid flow needed to be forces into the pipe system for heat transfer.

As previously mentioned, there was no pump that would fit the final design criteria due to the size constrains of the test bench. Designing a pump is difficult, given that there is a size constrain while having to maintain pump efficiency for optimum functionality. Our design has the requirements of 2 separate pumps, the hot exchange pump and the cold exchange pump.

8.4.1 Hot exchanger pump

The hot exchanger pump is one of the most complex components of the test bench. The general function that the pump must perform is moving the hot fluid. This must be done for 8 different heat exchangers. This increased complexity due to the fact that none of the 8 fluids can mix while running through the pump. Also, another key factor in the pump design is that there is a pre-heating stage in which the hot fluid from the heat exchanger is used in a regeneration stage to heat up a previously cold material. Due to the working nature of the pump, two impellers were required for the pump with 2 separate, isolated chambers. The pump itself is also designed to work of a central shaft powered by a single motor which gives power to every component of the test bench.

The pump consists of 2 separate chambers. The top chamber and bottom chamber work in unison, as the fluid must follow a constant path in a single direction. It may never reverse its

direction while maintaining separation from all other fluids. Figure 40 shows the top chamber without any of its inner workings, allowing for the inlet and outlet holes to be seen. These holes where designed to provide a given flow rate into and from the heat exchangers which was governed by

$$\dot{Q} = VA$$

Where $\dot{Q}$ the volumetric flow rate of the fluid, V is the fluid velocity, and A is the area.

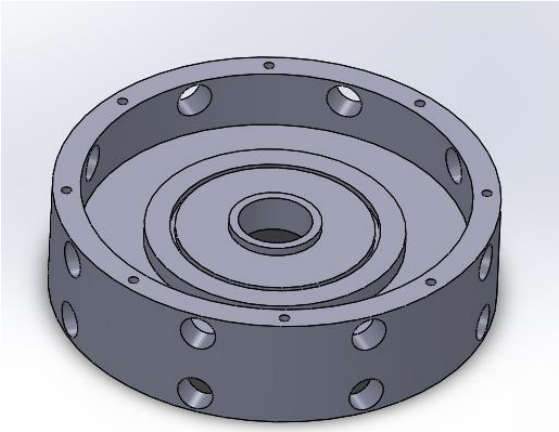

Figure 40: Top chamber

Due to the motor specifications, the maximum revolutions that the impeller will spin at is 120 RPM. This means that an average fluid velocity could be calculated by assuming that the fluid is incompressible. Finding an average velocity is done by

$$V = \omega * r$$

V is the average fluid velocity of the given displaced volume, omega is the angular velocity of the impeller, which in turn is the same velocity being transferred to the fluid due to the incompressibility assumption, r is the distance from the center of the drive shaft to the center of gravity of the displaced volume. Omega is calculated by converting the 120 rpms into radians/ seconds yielding 12.57 rad/s and an r of .0222 meters, giving an average velocity of the fluid of .279 m/s. For maximum heat exchange, the fluid flow must be turbulent to increase the heat transfer, so the minimum Reynolds number allowed is 4000. Reynolds number equation:

$$Re = \frac{\rho * v * D}{\mu}$$

By using a kinematic viscosity of .600e-3 Pa*s, due to an elevated temperature of 45°C, we have a final diameter of 9.36e-3 m (.368 in). This size is too large to implement into the pump so the only other option was to increase the rpm of the motor to 300 rpms and establishing the maximum diameter that the hole could be of .00635 m (.25 in), yielding a maximum average velocity of .6974 m/s and giving a maximum Reynolds number of 7380.

The test bench must vary rpms to find at what rpm the optimum cooling occurs so since the rpms vary, so will the Reynolds number. This meant that during the rpm variation, Reynolds number must stay above 4000. Again using the Reynolds number equation, knowing the diameter, viscosity and minimum Reynolds number we can calculate the minimum rpm that we can go and maintain turbulent flow. Running the calculations it yielded a velocity of.3779 m/s which translates to 17.02 rad/s, equaling to 162.53 rpms. These calculations allow us to vary parameters while maintaining the minimum acceptable flow.

The next key component of the top chamber of the pump is the channels. The channel is what allows for all eight flows to pass through the same pump and into their respective heat exchangers while maintaining flow separation. Figure 41 shows how the channel was designed to maintain flow separation but still be able to interact with the impeller for acceleration of the fluid. Designing the channel was critical because the channel size affects the volume displaced and also the port opening duration.

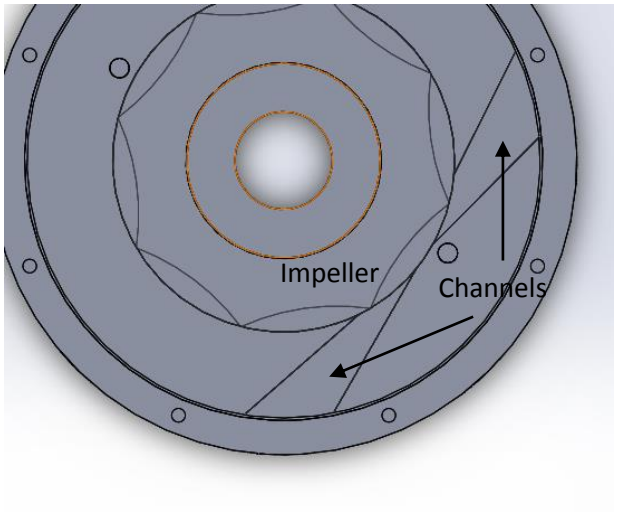

Figure 41: Channel

Extensive designing was done to allow for the maximum duration of the port opening while still marinating 0 overlap between one port hole and the next. Figure 42 shows the maximum value of 20° as being the key value that allowed maximum opening with 0 overlap.

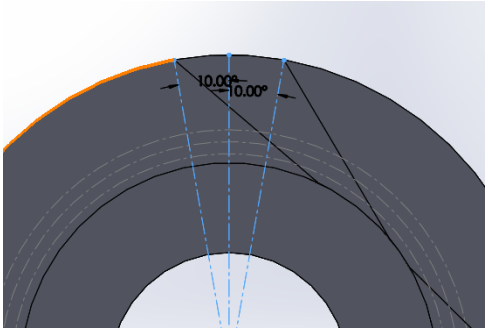

Figure 42: Opening duration

8.4.1.1 Pump Gears

The last element of the pump is the inner gears. The reason for inner gears is due to the fact that the impeller must spin at higher revolutions than the channel. If the channel were to spin at the same rpm as the impeller then there would be no fluid flow because the relative velocities between the channel and the impeller would be zero. Having a gear reduction of 2.8:1 ratio seemed suitable to allow for an acceptable opening duration of the port hole. The size constrain was huge only having 2.625 inches in diameter of space, minus the 1 inch that the impeller takes up. The reduction was rather high in comparison to the available space and many different types of gear trains were looked at, such as a compound gearing and epicyclical gears. The compound gearing was analyzed initially, but deemed unfeasible because of cost of nearly 20 gears to obtain the drop down ratio required. Also the size constrains limited the gearing position, which meant the gears, would have to circle around the impeller, making the design much more complex. Figure 44 shows the general form of a compound gear train and seeing that it would be very complex to fit inside the pump, as seen in figure 43.

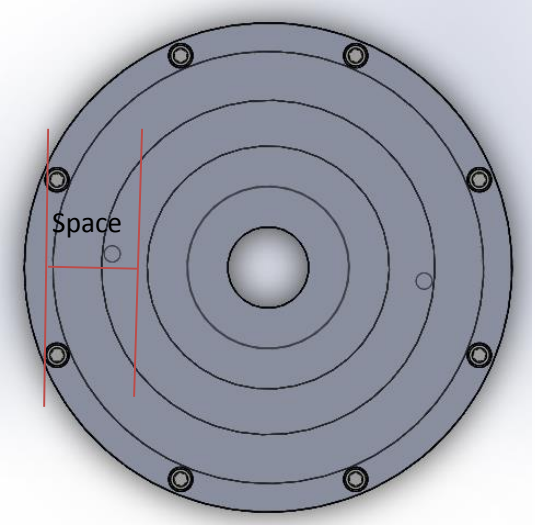

Figure 43: Gear spacing

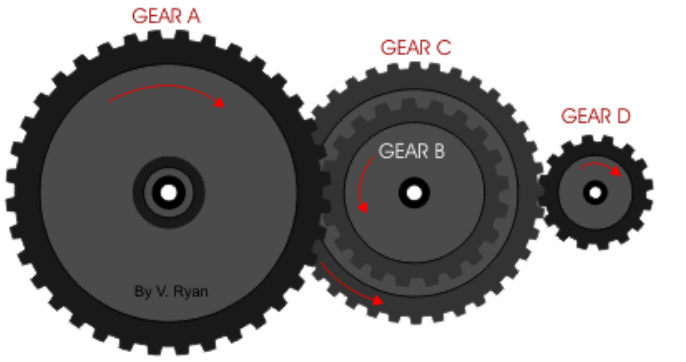

Figure 44: Compound gear train (Ryan, 2001)

The other gear train considered was epicyclical or, better known, a planetary gear train. The planetary gear train provides a larger drop in ratio in a more compact spacing than the compound gear train. Figure 45 shows the final design of the gearing inside the pump. The planetary gears consist of at least a sun gear, 2 to 3 planets and a ring gear. The planetary gear can have varying drop ratios according to the gear that is left stationary, for example the largest

drop is obtained by fixing the ring gear and the output would come from the planet rotation. The general equation for an epicyclical gear train is as follows

$$(R + S) * T_y = R * T_r + S * T_s$$

Where,

$$T_r = Turns\ of\ ring\ gear$$

$$T_s = Turns\ of\ sun\ gear$$

$$T_y = Turns\ of\ planet\ carrier$$

$$R = Ring\ gear\ teeth\ or\ diameter$$

$$S = Sun\ gear\ teeth\ or\ diameter$$

Fixing the ring gear yields,

$$R * T_r = -(S * T_s)$$

With the above equation, knowing how much of a gear drop required and fixing one of the 2 gear sizes allowed us to find the other gear size. After attaining general gear sizes, the number of teeth must be established per gear and insure that the gears will mesh together by having the same diametral pitch.

$$P = \frac{N}{d}$$

Where,

$$P = Diametral\ pitch$$

$$N = Number\ of\ teeth$$

$$d = Gear\ diameter$$

Varied diametric pitches where analyzed to establish a working number of teeth that would mesh with each other and also various working gear diameters. It is essential that the diameters used for each gear and diametral pitch will yield a whole number of teeth. Various calculations later a diametral pitch of 28 was achieved and suitable sizes that would fit in the pump, yielding table 7.

Gearing any component has some degree of complexity, as its not only about finding the teeth and pitch for the gears, but also assuring that the number of teeth have the minimum teeth size to avoid interference. The formula for the pinion is

$$N_p = \frac{2k}{(1+2p)sin^2\emptyset}(p + \sqrt{p^2 + (1+2p)sin^2\emptyset})$$

$$N_p = Pinion\ teeth$$

$$p = diametral\ pitch$$

$$k = teeth\ factor\ (1\ full\ teeth, .8\ stub\ teeth)$$

$$\emptyset = Pressure\ angle$$

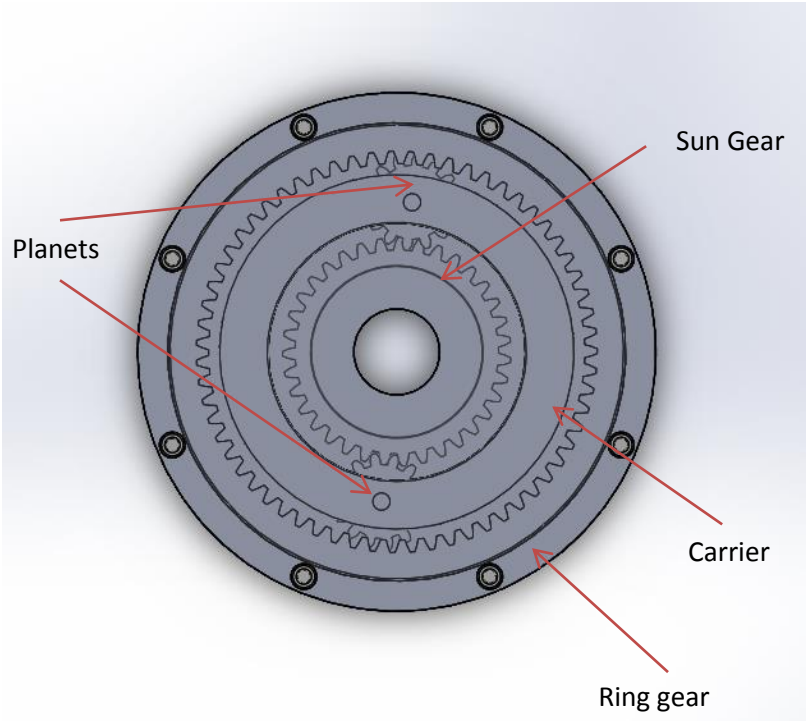

Figure 45: Epicyclic gear train

Epicyclical gear sizes and teet	Column	Column2
Gear	Teeth	Diameter(in)
Planet	14	0.5
Sun	35	1.25
Ring	63	2.25

Table 7: Epicyclical diameter and teeth

After finding the minimum teeth number for the pinion the same was done for the gear using the following equation

$$N_g = \frac{N_p^2 sin^2 \emptyset - 4k^2}{4k - 2N_p sin^2 \emptyset}$$

$$N_g = Gear\ teeth$$

$$N_p = Pinion\ teeth$$

$$k = teeth\ factor(1\ full\ teeth, .8\ stub\ teeth)$$

$$\emptyset = pressure\ angle$$

Using the above equations was determined that the current amount of teeth on each gear is higher than then minimum for interference. As seen in figure 45 the reason a carrier is needed is due to the number of teeth on each gear will not allow the planets to be positioned correctly. Looking closer at the location where the planet would have to mount to the channel, you would see that it ends up on the cut out of the channel, meaning mounting it there is impossible. The carrier was created so the planet could be positioned correctly while still maintain contact to the channel.

8.4.1.2 Gear stress

Gear stress is a very critical part of the gears that must be taken into account. The gears will be 3D printed meaning that it can easily shear through the layers. Due to this, the gear must be thicker and more robust to withstand the stresses.

The calculations begin by calculating the tangential force applied on a single tooth of the gear.

$$W^t = \frac{33000H}{V}$$

This equation only being valid for English units, where,

$$W^t = Tangental\ force\ (Lbf)$$

$$H = Power(HP)$$

$$V = pitch\ line\ velocity\ (\frac{ft}{\min}),$$

$$V = \frac{\pi d \omega}{12}$$

$$d = diameter\ (in)$$

$$\omega = \frac{rev}{min}$$

When the tangential force is calculated the equation for the bending stress is as follows

$$\sigma = W^t k_o k_v k_s \frac{P d K_m K_b}{F J}$$

The previously defined variables remain the same with

$$k = stressing\ factors\ (varying\ equations\ for\ each\ k)$$

$$P = dimetral\ Pitch$$

$$F = tooth\ face\ width$$

$$J = bending\ strength\ geometrical\ factor$$

$$k_m, k_b = Load\ distribution\ factor, rim\ thickness\ factor, respectively$$

This calculated bending stress must be used to find the safety factor or a safety factor can be set and see what the maximum bending stress is.

$$\sigma_{all} = \frac{S_t Y_n}{S_F K_t K_R}$$

$$\sigma_{all} = allowed\ stress$$

$$S_t = Allowable\ bending\ stress$$

$$S_F = Safety\ factor$$

$$Y_N = Stress\ cycles$$

$$K_T = Temperature\ factor (1 \leq 250°F)$$

$$K_R = Reliability\ factor$$

After finding the bending stress, the safety factor of the gear could be found by finding the allowable bending stress. This value will be found according to the material being used, which in this case is abs plastic. According to table 18.1 from Design of plastic gears (QTC Gears, 2013) the abs plastic has a tensile strength of 4.5 – 8.5 x 10^3 psi. By knowing the tensile strength you can plug this value as the maximum strength and the calculated bending stress equation, the equation for maximum bending stress equation will be solved for safety factor.

$$S_f = \frac{S_t Y_n}{K_T K_R \sigma}$$

The next calculation that must be performed on the gears is to make sure there will not be failure due to wear on the gear. The wear stress on the gear is found by

$$\sigma_c = C_p(W^t K_o K_v K_s \frac{K_m C_f}{d_p F I})^{1/2}$$

Where,

$$\sigma_c = Contact\ stress$$

$$C_p = Elastic\ coefficient$$

$$I = Surface\ strength\ geometry\ factor$$

The rest of the nomenclature has been previously stated. From the wear stress then the factor of safety can be calculated by

$$\sigma_{c,all} = \frac{S_c Z_n C_h}{S_h K_t K_R}$$

Where,

$$S_c = allowable\ contact\ stress$$

$$Z_n = Stress\ cycle\ factor$$

$$C_h = Hardness\ ratio\ factor$$

$$S_h = Contact\ factor\ of\ safety$$

After all the calculations were performed, the values can be seen in table 8, which would show that the gears will not fail after substantial usage and wear. By comparing the safety factors we can see that the failure will be due to fatigue on the teeth, due to bending stress and not the contact stress. The gear analysis for the cold exchanger pump is the same as the hot pump as they have the same internal gears.

Table 8: Gear stresses and safety factor

Gear	Bending Stress	Safety Factor	Wear stress	Safety Factor2
Planets	2406.96	1.87	4164.05	3.48
Sun	1643.28	2.75	1716.33	8.45
Ring	660.93	6.84	969.7	14.96

The factor of safety seen in table 8 would actually be lower than calculated because of the manufacturing method of the gears. The gears due to cost are 3D printed from ABS plastics;

however, according the calculations assumed these formulas do not take into account how the product is layered during the printing process. The 3D printing is very cost effective for manufacturing, but it sacrifices the integrity of the piece by layering, which they are prone to a lot of shear stresses that could break the gears. This is a factor that was taken into consideration when designing the gears by having a larger face width on the gear and also the cost vs. wear of the gear allows for multiple pieces to be printed for the cost of a single metal gear.

8.4.2 Cold exchanger pump

The cold exchanger pump has the same working internals as the hot exchanger pump. The difference between the cold and the hot exchanger pump is that the cold pump has a single impeller, unlike the dual impeller of the hot pump. A single impeller pump is allowed for the cold exchanger pump because the flow can mix inside the pump without any repercussion to the efficiency. The assembled pump can be seen in figure 46 how it has dual chambers, the upper half is the impeller and the lower half is a fluid reservoir, which would pump the water into the impeller to be accelerated into the heat exchangers. The top chamber with the impeller functions very similar to the hot exchanger pump, the difference is that the channels of the cold exchanger pump are not channels, but rather a series of opening which open and close various port holes. The channel can be seen in figure 47 how it opens and closes the port holes on opposite sides of each other. The cold pump also has its own timing, just like the hot pump does. The fluid in the bottom chamber gets pumped up to the impeller with a submergible electric pump. The cold pump is a much simpler design than the hot pump since there where less constrains in the design.

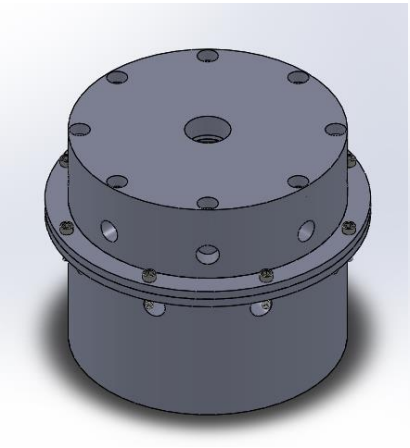

Figure 46: Cold exchanger pump

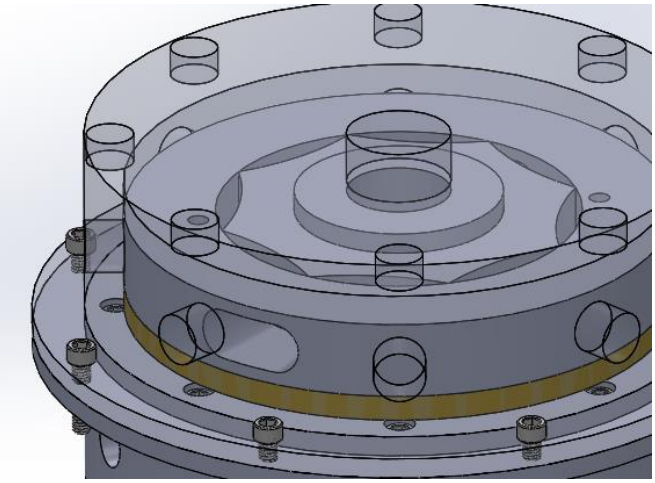

Figure 47: Cold Pump Channel

8.5 Cams

8.5.1 Cam Design

The cam is a critical component of the magnetocaloric test bench, as it's what allows for the heat exchangers to actuate and make contact with the material. The original design was based of pneumatic actuators that would be controlled by the Arduino. Due to cost of the actuators and various valves needed for the design to work properly, the design was scraped. The latest cam design is seen in (Cam in assembly) with the whole assembly. This design is a simple cam actuation and the heat exchangers follow the cam with a roller. The cam is attached to the outer magnet assembly and will have the same revolutions as the outer magnets. The simplification from the previous design allowed for a lower cost and allowed for the cam to run of the main shaft as every other component in the assembly.

The cam material was chosen to be aluminum since it would be fixed to the outer magnet holder. The cam follows a circular path which meant that an aluminum cam would be out of budget due to the manufacturing cost, since a 6 axis CNC would be required. The design remained the same but 3D printing the cam was looked at. The advantages was that any design could easily be printed and would be substantially cheaper than the aluminum counterpart. The disadvantage was that since the 3d printer deposits the material in layers, it was not clear if the material would sustain the shear stresses of the cam actuation when spinning at 107 RPM's.

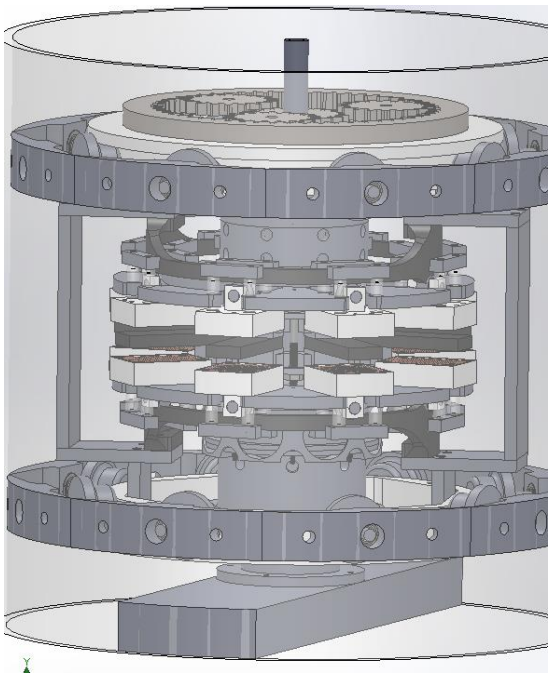

Cam in assembly

Looking at the shear stresses that the cam will sustain, we began by finding the max allowable strain that ABS plastic can sustain. The value is 4% elongation and a 328510 Psi young's modulus.(1) The basic shear stress equation is:

$$\tau = \frac{F_p}{A}$$

Where,

$$\tau = Shear\ stress$$

$$F_p = Parallel\ Component\ force$$

$$A = Area$$

With the strain equation we can calculate the largest shear stress that the piece can sustain before failure.

$$\varepsilon = \frac{\Delta L}{L} = \frac{\sigma}{E}$$

Where,

$$\varepsilon = Strain$$

$$E = Youngs\ Modulus$$

The maximum stress is calculated to be 1314.04 Psi, which would mean that using the previous stated equation for stress we can find the maximum force before failure. Using the smallest area of shear, which could be seen in (cam), the shear area is .259 in^2, yielding a maximum force of 340.33 Lbs. This force is the largest force before failure and this is not allowable for the design. A design stress must be determined which making an assumption for it to be

$$S_{ys} = .5\, S_y$$

Where,

$$S_{ys} = Yield\ strength\ in\ shear$$

$$S_y = Yield\ stress\ in\ tension$$

Calculating the yield strength gives 7542 Psi, dividing the maximum stress experienced by the cam yields a safety factor of 5.73. This safety factor does not take into account the cyclic loading, so by good engineering judgment the yield strength is cut by a factor of .5 yielding a final safety factor for the cam of 2.87.

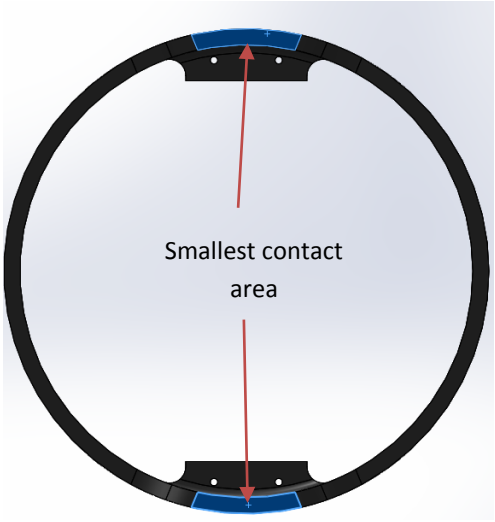

cam

8.5.2 Cam Timing

The cam timing is very critical to the function of the Magnetocaloric test bench. After the material is Magnetized the hot heat exchanger must come down at the correct time, which would allow the largest contact time, while maintain feasibility of the cams. At the moment of demagnetization the cold heat exchanger must come into contact with the material to obtain the highest heat transfer possible.

(Hot Cam) shows how the timing offset has to be 29.28° for the heat exchanger to be actuated as soon as the material is undergoing constant magnetization. The largest contact time is due to the largest contact area seen in (cam), which has a total size of 26.2°. Since the contact area is smaller than the magnetization stage, the cam timing is set up for the hot heat exchanger to be in contact right up to the time it gets demagnetized, which at that time the cold heat exchanger will actuate and contact the material. The cold heat exchanger will have a 60° offset when measured from the same reference as the hot exchanger cams as seen in (cold cams).

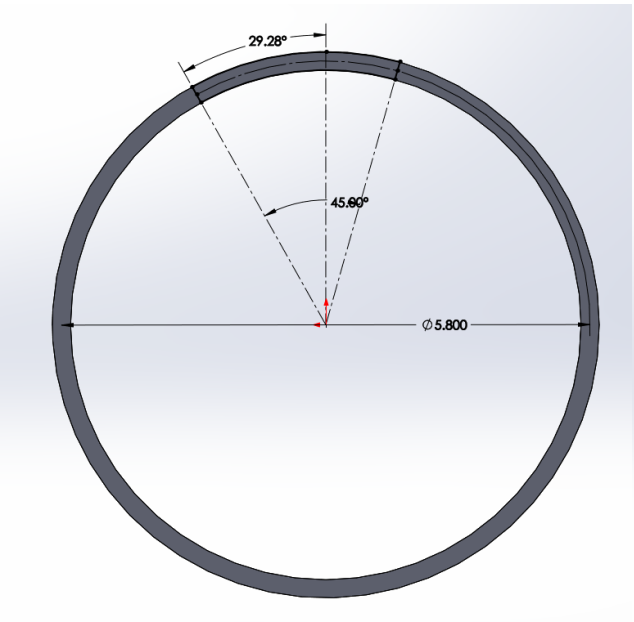

Hot Cam

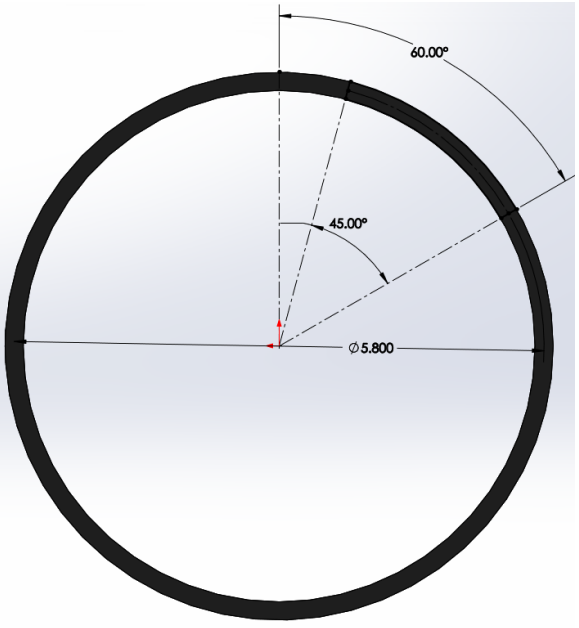

Cold Cam

9. Project Management

9.1 Labor and Time Management

Table 9 shows a Gantt chart depicting the major phases of the project as well as the delegation of work divided amongst the team members. The product fabrication was a key factor in being able to finish the project. About 95% of the project was machined by the team, since most of the project was custom made pieces. This increased our machining time and how long the prototype took to make. The manufacturing also tied into the cost since most of the prototype is a one off piece, the cost increased substantially.

Table 9: Project Timeline & Division of Labor

Task Name	Members	Start Date	End Date
Magnetocaloric Refrigeration		01/07/13	11/22/13
Project Formulation	EG-ML-FI	01/07/13	02/06/13
Research & Development	EG-ML-FI	02/06/13	05/31/13
Conceptual Design	ML-FI	03/11/13	04/19/13
CAD Model	EG	04/01/13	04/19/13
Software Simulation	ML-FI	04/15/13	04/25/13
Proof of Concept	ML	04/30/13	05/14/13
Design Optimization	EG-ML-FI	05/01/13	05/29/13
Component Testing	FI	06/01/13	07/05/13
Prototype Fabrication	EG-ML-FI	07/01/13	09/27/13
Prototype Testing	EG-ML-FI	08/26/13	10/18/13
Prototype Optimization	EG-ML-FI	09/23/13	11/08/13
Final Report	EG-ML-FI	07/01/13	11/22/13

9.2 Cost Analysis

In determining the cost for the development of the magnetocaloric effect testing apparatus, three categories which would best sum up and take into account the amount of work and cost necessary are as follows:

- Travel
- Materials
- Manufacturing

9.2.1 Travel

This category involved investing in round trip to Ames, Iowa for all E-Mech team members. The flight to Iowa was proposed in order to greet and meet the members responsible for a similar MCR cycle stationed at the Ames Laboratory. Generally, this idea was primarily used to motivate and facilitate growth in team spirits in order to build a common interest for the task of developing the MCE tester. Visiting the Ames Laboratory would also provided deeper understanding on the subject, servicing as a reference aid in development of the MCR cycle.

9.2.2 Materials

The bulk of total cost in designing and prototyping E-Mech's MCR system is taken up mostly by this category. Various metals and machines such as motors as well as circuit boards are included in this cost analysis. All materials will, with the exception of the working MC material, are purchased through various distributors across the United States. Some of these distributors include Speedy Metals, McMaster, and Online Metals. The most expensive piece of material taken into consideration above all other accompanying components are the previously mentioned curved copper tubing, seeing as thought the alloyed copper tube has a relatively high market value. The next costly items to consider in terms of importance are the hot and cold heat exchangers for which there is only one of each. In the case where either of the these components is to ultimately fail or become unusable, although relatively low in price, the resultant cost for disassembly and reassembly of the system in reinstalling the heat exchangers would require the purchase of additional copper tubing in addition to purchasing new heat exchangers. Thus, the

value of importance that each major component contributes to the cooling system greatly affects and directly links to the total monetary value of the design.

The initial cost of the design used the best components and materials for the best results possible. This included pre-made heat exchangers from water cooler computers, every component being made out of T6 aluminum and many components where high quality parts. With the initial design the prototype was going to run of budget, so various changes had to be made. Much of the prototype was changed from metal to plastics ranging from self-lubricating Nylon to 3D printed ABS plastic. This allowed for the cost to drop substantially and it allowed the project to stay within budget.

9.3.3 Manufacturing

There are certain accommodations unique to the final design of the MCR cycle that requires customized manufacturing of specific components. In this case, the cost in manufacturing these pieces increases in addition to the purchased price for the material itself. Examples such as these are found in other components of the cooling system that have small, detailed and or complex geometric features. Although this challenge increases the resultant cost, precise and professional custom manufacturing reduces the work load and relaxes the amount of tasks toward completing the task of prototyping the MCE tester prototype.

Table 10 is the representation of the approximate cost analysis taken from the trip and materials section which includes only general information of the major components used in the MCE tester design.

Table 10: Projected Estimated Cost of Project

Travel			
Description	Qty.	Price (EA)	Total
Round Trip	3	$648.00	$1,944.00
Material			
Description	Qty.	Price (EA)	Total
Copper Tube **ID**: 3in - **L**: 4ft	1	$489.00	$489.00
Copper Tube **OD**: 3.5in - **L**: 4ft	1	$200.00	$200.00
Copper Tubing	2	$50.00	$100.00
Copper sheet	2	$100.00	$200.00
Steel sheets	1	$80.00	$80.00
Hot Heat Exchanger	1	$200.00	$200.00
Cold Heat Exchanger	1	$200.00	$200.00
Pump	1	$150.00	$150.00
Motors	1	$30.00	$30.00
Arduino	1	$80.00	$80.00
Thermocouples	4	$30.00	$120.00
Total Estimated Cost			$1,849.00

The physical cost of research, design, and prototyping as opposed to the financial aspect of the project is also taken into account. This analysis gathers, in detail, the number of hours dedicated into and up to the development of the Magnetocaloric Effect Tester. Generally, this time study may very well simulate the amount of work hours in an industrial-type setting. Table 11 illustrates, in detail, the collective project hours dedicated to the MCE Tester.

Table 11: Projected Time Spent on Project

Category	Task	Hours	Total Hours
Research	MCE Applications	4	61
	MCE Materials	8	
	MCE Process	18	
	MCR Components	15	
	MCR Designs	8	
	Trip: Ames Labs, Iowa	8	
Design	Individual Concept Design	15	129
	Team Design Meeting	30	
	Design of Mount Station	8	
	Final Design	10	
	Design of Chambers	8	
	Design of Heat Exchangers	8	
	Design of Enclosure	4	
	Design of Test Piece Implementation	8	
	Design of Arduino Implementation	12	
	Design of Temperature Reading	6	
	CAD Modeling	20	
Prototyping	CAD Simulations	15	128
	Construction of MCE Station Mount	6	
	Construction of MCE Chambers	24	
	Modification of Heat Exchangers	8	
	Construct Material Mount	8	
	Build Circuit	20	
	Building The Enclosure	12	
	Installing Thermocouples	3	
	Test Apparatus	20	
	Modifications to Apparatus	12	
Reports & presentation	Senior Report	40	77
	Presentations	20	
	Rehearsals	4	
	Drawings	3	
	Poster	10	
Total Amount of Hours			395

In response to the projected cost of the project, an actual cost analysis is constructed for comparison consisting of several parts, components, and tooling necessary for the project build. Table 12 lists what is considered the major items essential to the final design. The cost and resultant cost are also listed respectively.

Table 12: Major Parts & Components

Major Parts & Components		*Qty*	*Cost*
Motor	300 RPM geared motor	1	$38.82
	Central Shaft	1	$10.38
Pumps	Structure Material	1	$52.22
Magnets	Magnet Holder	1	$9.71
	Rail	2	$136.78
	Roller Wheels	3	$27.03
	Magnets	250	$87.50
Outer Tube	Clear Acrylic Tube	1	$191.00
	Rail Holder	2	$28.36
Test Material	Holder	1	$93.86
	Clamping Ring	1	$7.14
Heat	Structure Material	1	$44.72
Exchangers	Springs	64	$136.13
	Copper Plates	4	$63.96
		Total Amount	$927.61

Other than the major parts and components, there are what is considered minor parts and components. Table 13 lists the items that were primarily used in accompaniment to the major items.

Table 13: Minor Parts & Components

Minor Parts & Components		*Qty*	*Cost*
Pumps	Impeller Bearings	4	$3.84
	Channel Bearings	3	$5.64
	Gear Dowel Pins	8	$11.44
	Binding Posts	1	$10.55
	Collar	2	$2.44
	Threaded Adapters	38	$13.04
	Submergable Pump	1	$11.99
	Shaft Seals	1	$4.74
Magnets	hose	25	$3.50
Test Material	Bearing	16	$117.28
	Nuts	6	$22.98
Heat Exchanger	Set Screw	4	$22.04
	Guide Pins	6	$3.90
	Copper Plate Bolt	3	$15.00
	Topper Guide Pin	1	$8.14
	Wheel	1	$1.63
	Total Amount		$258.15

The following items to consider was tooling for machining and or altering and assembling both the major and minor parts and components. Table 14 illustrates the necessary tools purchased.

Table 14: Tooling Costs

Tooling	*Qty*	*Cost*
right hand lathe 1/2 shank	2	$11.66
1/4" Diam, 1" Cutting, 2 flute	2	$39.10
1/8" diam, 3/8" cutting 2 flute	1	$22.27
.05" diam regular length 2 flute	1	$18.88
.04 diam regular length 2 flute	1	$19.41
.07 diam drill bit #50	1	$1.56
.152 diam #24	1	$1.81
.228 diam #1	1	$2.80
.1015 diam #38	1	$1.56
1/4 diam bit	1	$2.80
1/2 diam bit	1	$10.79
1/8 diam bit	1	$1.53
.14 diam #28 bit	1	$1.56
.089 diam #43 bit	1	$1.56
.1065 diam #36 bit	1	$1.56
.166 diam #19 bit	1	$1.97
2-64 tap	1	$1.56
4-48 tap	1	$1.56
2-56 tap	1	$1.56
4-40 tap	1	$6.13
10-32 tap	1	$4.96
11/16 diam bit	1	$29.41
.185 diam #13 bit	1	$2.25
.1130 diam #33 bit	1	$1.56
3/32 diam bit	1	$1.40
.0935 diam #42 bit	1	$1.56
.238 diam B bit	1	$3.31
.086 diam #44 bit	1	$1.56
.199 diam #8 bit	1	$2.33
Total Amount		$199.97

The total amount referenced by Tables 12, 13, and 14 sum up to a grand total of about $1,385.73. With a Budget amount of about 1,500, this provided a difference of $114 for miscellaneous purposes towards the completion of the design.

Several manufacturing methods were implemented during the fabrication of this project. Amongst these are rapid prototyping, manual machining, and CNC machining. The majority of the device was designed using plastic composites in order to reduce material and manufacturing costs. There were, however, a few parts that had to be redesigned due to unacceptable finishes caused by small size. The plastics used can be seen in Table 15 along with several of their properties which affect manufacturability.

Table 15: Plastic Specifications

Material	Tensile Strength (psi)	Rockwell Hardness	Impact Strength (ft*lbs/in)	Coefficient of Friction	Density (lbs/in^3)	Machine With
UHMW Polyethylene	2470 - 7740	Shore D61-D77	16.8 – No Break	0.12 - 0.25	0.034	HSS
LDPE Polyethylene	3100 - 6100	Shore D42-D56	Not Rated	Not Rated	0.033	HSS
Delrin Acetal Resin	9000 - 11000	M89 - M94	1 - 2.4	0.2	0.051	HSS
Glass Filled Polycarbonate	16000	Not Rated	2.06	Not Rated	0.048	Carbide
ABS	5100 - 6100	R102 - 109	5.2 - 7.7	Not Rated	0.032 - 0.038	HSS

The table shows that the majority of the materials can be machined with high speed steel with the exception of the Glass Filled Carbonate. This allowed for the reuse of tooling which in turn reduced cost.

Parts that were exhibited to negligible loads were rapid prototyped. The material used was ABS plastic and solid mesh was implemented in the printing. The solid mesh was chosen due to the rigidity and durability it provided to the parts. The cost of the extra material necessary for the solid mesh was negligible when compared to the benefits of choosing this design. The device used to print the parts was a Solidoodle which can print within an 8” x 8” x 8” cube. The device can be seen in Figure 48.

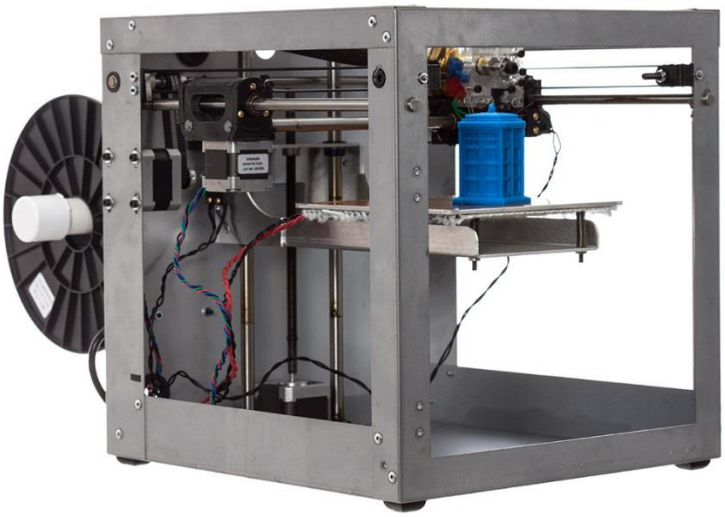

Figure 48: Solidoodle 3D Printer

Machining for parts such as the heat exchanger were performed on a knee mill. A half inch two flute flat end mill was used for this. This provided the team with the dimensioning necessary as well as reduced machine time. Different parts called for different tooling. Another machine used was a lathe. It was used to turn circular components. Standard high speed steel tools were used. Turning the parts at an average 1300 RPM and applying coolant caused very little tool wear and reduced tooling cost drastically. The left of figure __ shows a hole being machined into a piece of aluminum using the knee mill and the right side shows a piece of plastic being turned on the lathe.

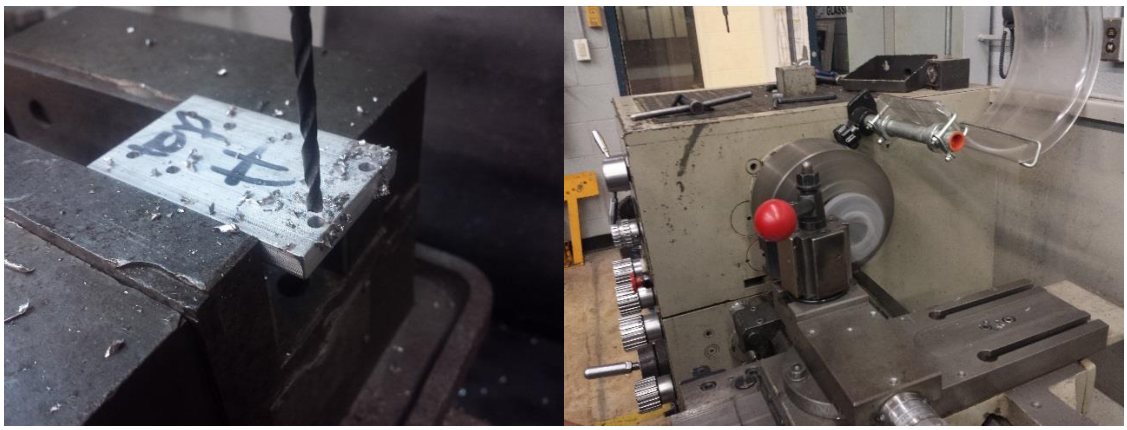

Figure 49: Knee Mill drilling hole (left), Lathe turning plastic (right)

10. References

Bartlett, D. A. (1996). The Fundamentals of Heat Exchangers. *The Industrial Physicist*, 18-21.

Bjørk, R. (2010). *Designing a magnet for.* Denmark: Riso DTU.

Bruck, E. (2010). Magnetocaloric Materials for Room-Temperature Applications. *FUndamental Aspects of Materials and Energy*.

D. Baldomir a, b. J. (2007). Magnetic field dependence of the magnetocaloric effect in magnetic. *Journal of Non-Crystalline Solids 353*, 793-795.

D. Liu, M. Y. (2009). Origin and tuning of the magnetocaloric effect for the magnetic refrigerant MnFe(P1-xGex). *Physical Review B. Vol. 79*, 1.

Elie Tawil, P. (1993). *Centrifugal and Positive Displacement Pumps.* Stony Point: Continuing Education and Development, Inc.

Gunther Gridling, B. W. (2007). *Introduction to Microcontrollers.* Vienna: Vienna University of Technology.

H. SZYMCZAK*, R. S. (2008). Magnetocaloric effect. Physics and applications. *Materials Science-Poland, Vol. 26*, 807-814.

Jacobsen, C. B. (2002). *The Centrifugal Pump.* Brookshire: GRUNDFOS.

Kevin D. Rafferty, P. (1992). Heat Exchangers. *Geo-Heat Center*, 261-277.

LLC, N. I. (2007). *Permanent Magnet Selection Handbook.* Vienna: Magcraft.

Magcraft. (2013). *MAGCRAFT - Advanced Magnetic Materials*. Retrieved 04 09, 2013, from http://www.rare-earth-magnets.com/p-6-nsn0566.aspx

Parker, D. B. (1994). *POSITIVE DISPLACEMENT PUMPS-PERFORMANCE AND APPLICATION.* College Station: Texas A&M University.

QTC Gears. (2013). Retrieved September 20, 2013, from qtcgears.com: http://www.qtcgears.com/q410/pdf/techsec18.pdf

Ryan, V. (2001). *Compound Gear*. Retrieved September 20, 2013, from Techologystudent.com: http://www.technologystudent.com/gears1/gears3.htm

Ucke, H. J. (2004). A fast, high-tech, low cost electric motor construction. *Physik in unserer Zeit 35*, 272-273.

V. K. Pecharsky and K. A. Gschneidner, J. (1997). Giant Magnetocaloric Effect in Gd5sSi2Ge2d. *PHY S I CAL REV I EW LETTERS*, 4494-4497.

Zhang, M. (2010). *Research and Implement of Thermocouple Sensor and Microcontroller Interface.* Huaihai: Huaihai Institute of Technology.

Discussion

The goal of this project was to design and manufacture a test bench. The test bench was to read temperature fluctuations of a designated material. The purpose of this was to determine the maximum temperature change (Δt) of Magnetocaloric test specimens. Magnetocaloric materials are materials which exhibit temperature changes when exposed to a magnetic field. The overall goal of the test bench was to expose the material specimens to magnetic field in such a manner where a refrigeration cycle would occur. The timing of magnetization and demagnetization, coupled with adiabatic heat removal, was key to achieving the desired behavior from the material.

Mainstream refrigeration technology takes advantage of certain properties of specific gases. These gases are typically fluorocarbon and chlorofluorocarbon based. The problem with these gases is that they are damaging to the environment. Magnetic refrigeration will potentially remove the need for these gases as well as the need for expensive compressors. The major hurdle in making magnetic refrigeration mainstream is the cost of Magnetocaloric materials. Gathering data for ferrous polycrystalline materials will result in the development of cost friendly Magnetocaloric materials and was the overall goal of this test bench. Eradicating the need for gaseous coolant solves the issue of potential coolant leaks. This implication is priceless in many applications. For example, removing the possibility of coolant leaks on the international space station would result in a decrease in the number of expensive and dangerous space walks.

The major design constraint for the project was to have the entire system work off of a single rotating shaft. This opens doors for having efficient magnetic refrigeration systems where tight packaging constraints are a concern as well as transferring rotational energy from an existing system that may need cooling. An example of this is automobile applications where a negligible amount of rotational energy can be drawn from the engine's crankshaft. One of the challenges encountered due to this constraint was designing pumps which would channel coolant while synchronizing with the timing of the magnetization and demagnetization of the

test specimens. Pre-manufactured pumps were out of the question due to geometrical constraints and the energy source being a central shaft. Each pump has an inner gear train in order to achieve a 2.8:1 reduction to the channel which diverges the coolant to its respective heat exchanger. Several other gear trains were used in order to reduce the rotation of the shaft to the rotation of the magnets. The ratio was maintained at a constant 2.8:1 in order to synchronize the timing off the entire system.

The initial design consisted of mostly aluminum. This choice was made due to the easy machinability of aluminum as well as its ability to maintain tight tolerances. Due to tight packaging of small parts, the ability to hold design tolerances within 0.01” was crucial. This tolerance was calculated by performing tolerance stack analyses. In order to stay within the design budget for the project, the majority of the material was changed to plastic. Low density polyethylene and Delrin Acetal Resin were chosen after performing a static loading analysis of each part. This change increased machine time due to slower feed rates. The feed rates were slowed down in order to hold the necessary tolerances while performing manual machining. This change also decreased the overall material cost by 30%.

Data acquisition was performed via an Arduino microcontroller. The controller supplied power to the motor as well as the logic for gathering voltage readings from 8 thermocouples and converting those readings into temperatures. These temperature readings are crucial in understanding the effect that the magnetic field has on the material specimens. They will be used to develop cost efficient polycrystalline materials which exhibit a high Magnetocaloric effect.

Appendices

Appendix A: Detailed Raw Design Calculations and Analysis

A.1 System Gear Reduction

The following Computations were tabulated using already established methods for mechanical systems as described in Shigley's Mechanical Design text book.

Minimum Number of Teeth: $N = \frac{2k}{(1+2m)\sin^2\phi}\left(m + \sqrt{m^2 + (1+2m)\sin^2\phi}\right)$

- k = 1 (crown tooth)
- m = 2.8 (reduction module)
- $\phi = 20^\circ$ (pressure angle)

$$\frac{N_{ring}}{N_{sun}} = m = 2.8 \quad \rightarrow \quad N_{sun} = \frac{2(1)}{(1+2(2.8))\sin^2 20}\left(2.8 + \sqrt{2.8^2 + (1+2(2.8))\sin^2 20}\right)$$

$N_{sun} = 15\ teeth\ (rounded\ up)$ $\qquad d = \frac{N}{P}$

Governing Equation = $\frac{d_{ring}}{2} = \frac{d_{sun}}{2} + d_{planet}$

- d = Diameter
- N = number of teeth of the gear
- P = 5 teeth/in diametral Pitch

Gear Selection						
Sun Gear	Nsun	20 teeth	d	2 in	P	5 teeth/in
Ring Gear	Nring	56 teeth	P	5 teeth/in	d	5.6 in
Planet Gear	Nplanet	18 teeth	P	1.8 teeth/in	d	1.8 in

A.2 Pump Gear Reduction and Stress Analysis

Ratio 2.8:1

P = 28 teeth/in

Gear Selection				
Sun Gear	d	1.25 in	N	35 teeth
Ring Gear	d	2.4 in	N	63 teeth
Planet Gear	d	0.5 in	N	14 teeth

Gear Stress based on AGMA standards: Sun Gear

Stress:

$$\sigma = W^t K_0 K_v K_s \frac{P d K_m K_b}{F J}$$

W^t [lbf]	2.25	J	0.35
K0	1.25	P	28
Kv	1.135	d	1.25
Ks	0.8914	Kb	1

σ = 1,643.28 psi Safety Factor = $\frac{S_t Y_N}{K_t K_R \sigma}$

St	5x10^3	Kt	1
Yn	0.8	Kr	0.885

S.F. = 2.75

Wear:

$$\sigma_c = C_p \left(W^t K_0 K_v K_s \frac{K_m C_f}{d_p F I} \right)^{\frac{1}{2}}$$

Wt	2.25	Kv	1.135
Km	1.155	Cf	1
K0	1.25	Ks	0.8914
F	0.2	Cp	245.97
I		0.27	

$\sigma_c = 1{,}716.33\ psi$ $S_H = \frac{S_c Z_H C_H}{K_t K_R \sigma_c}$

Sc	18900	Kt	1	Zn	0.6791
Ch	1	Kr	0.885		

$S_H = 8.45$

Following the same procedure for the planet and ring gear...

Gear Stress based on AGMA standards: Planet Gear

Stress:

σ = 2,406.96 psi S.F. = 1.87

Wear:

σ_C = 4,164.05 psi S_H = 3.48

Gear Stress based on AGMA standards: Ring Gear

Stress:

σ = 660.93 psi S.F. = 6.84

Wear:

σ_C = 969.7 psi S_H = 14.96

Appendix B: Major Component Engineering Drawings

B.1 Pumps

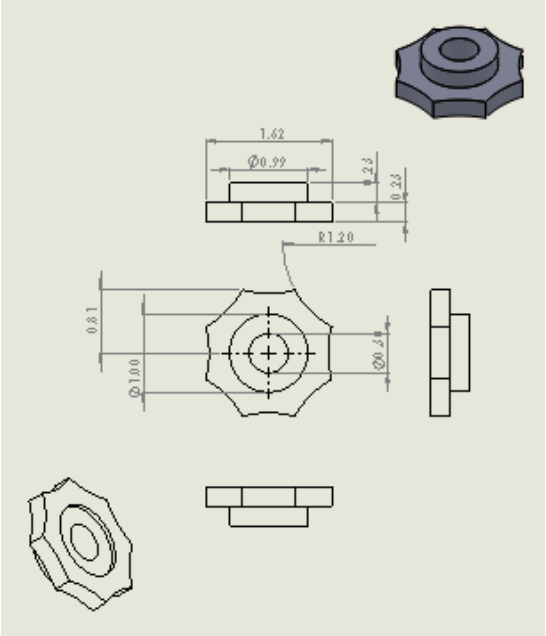

Figure 50: Hot Pump Impeller

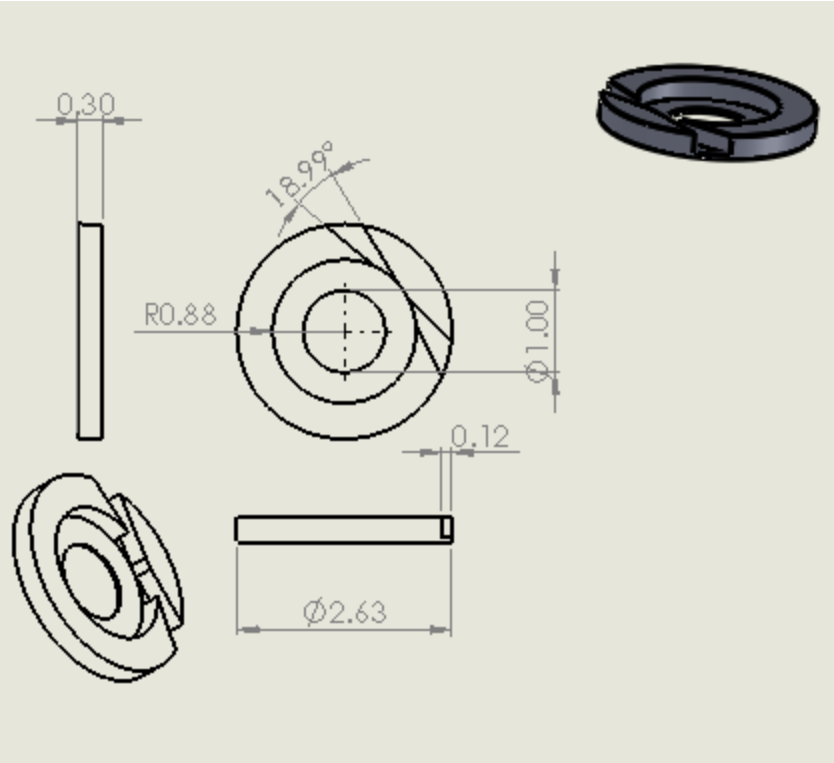

Figure 51: Hot Pump Channel

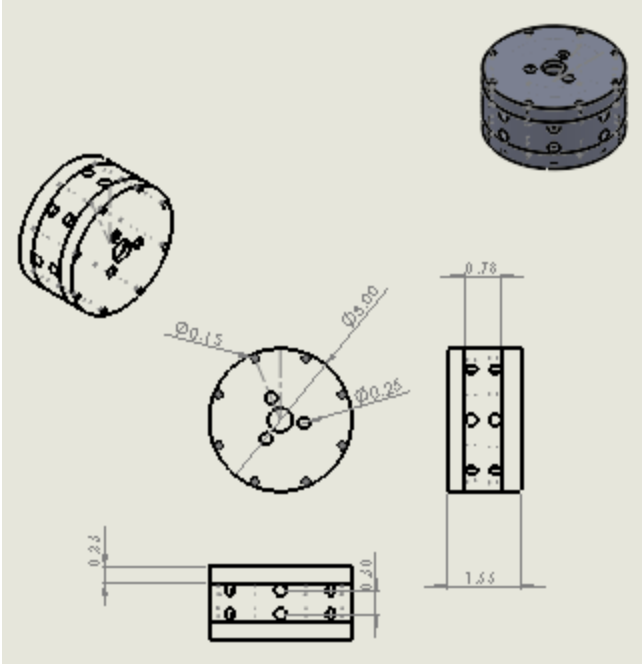

Figure 52: Hot Pump Assembled

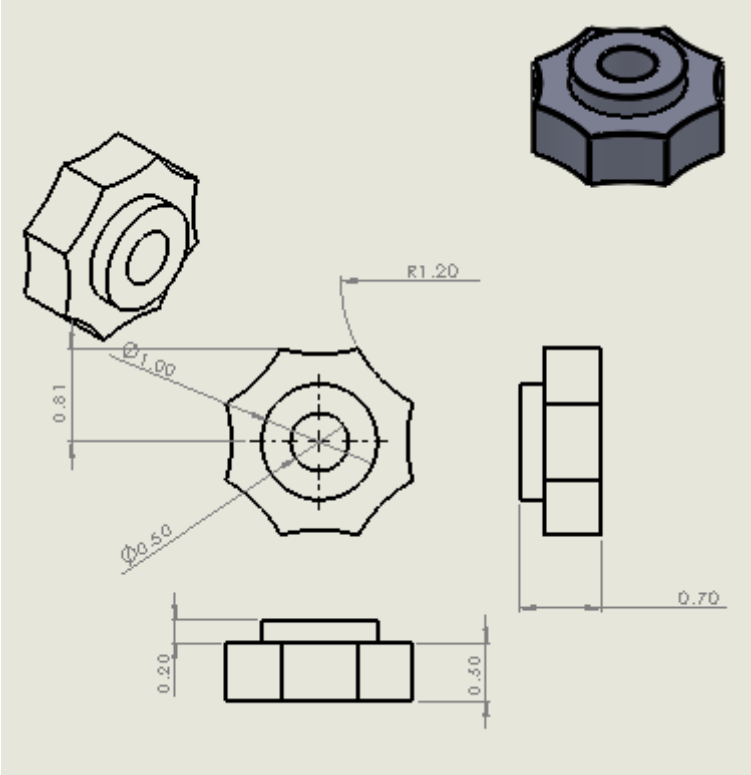

Figure 53: Cold Pump Impeller

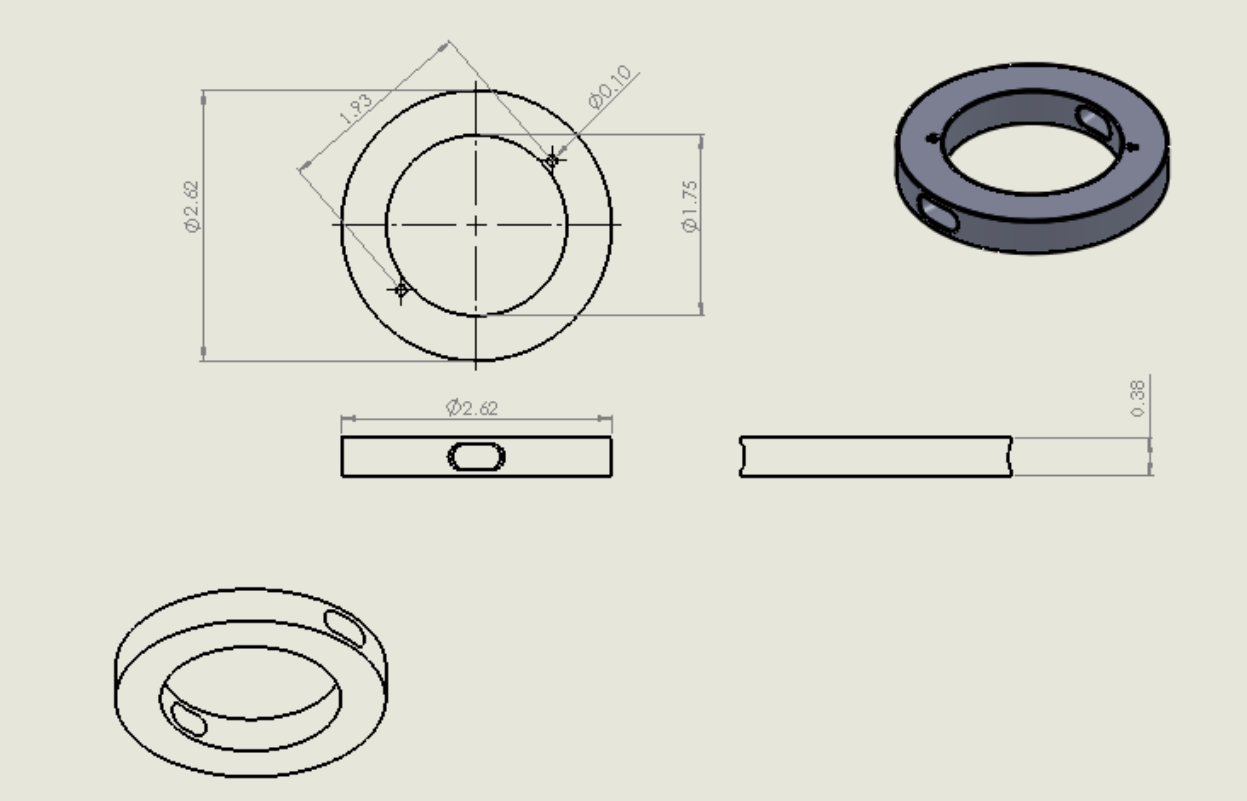

Figure 54: Cold Pump Channel

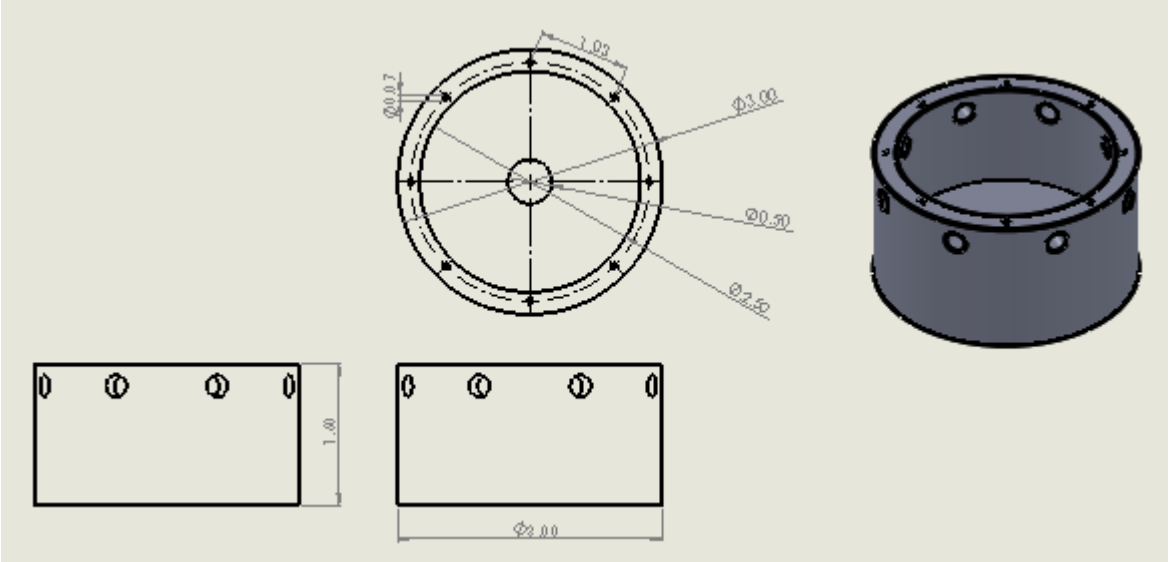

Figure 55: Cold Pump Reservoir

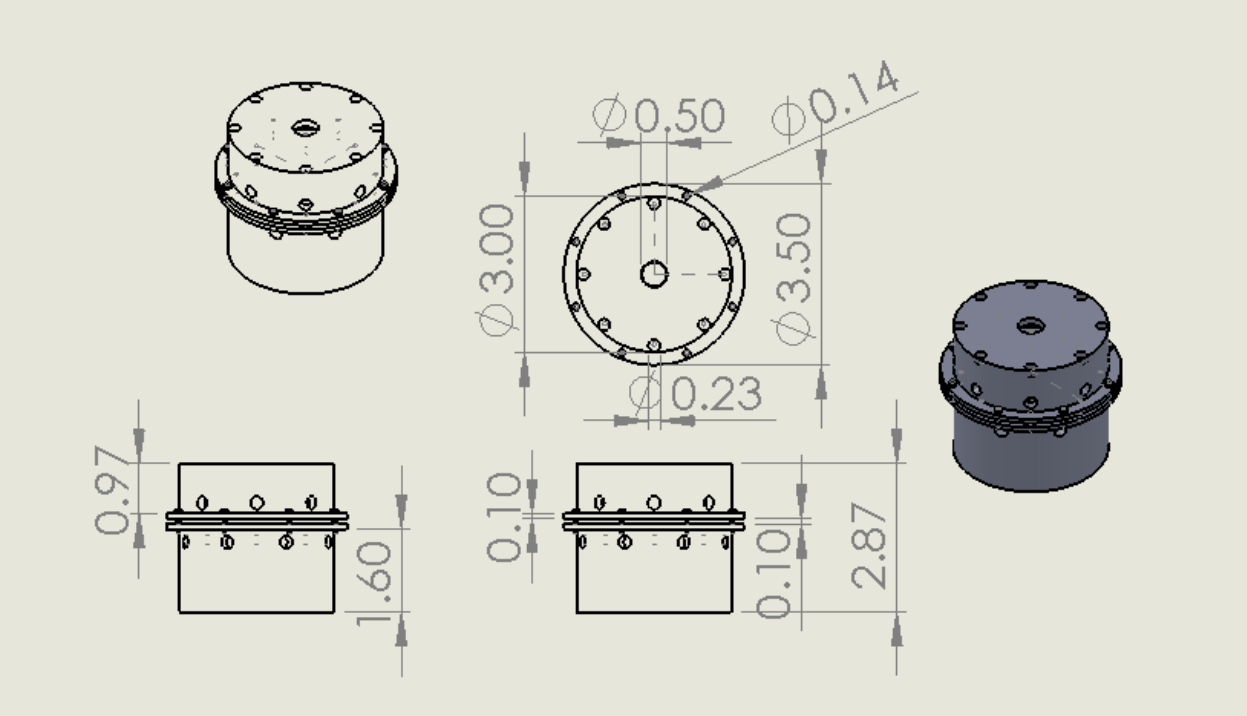

Figure 56: Cold Pump Assembled

B.2 Heat Exchanger

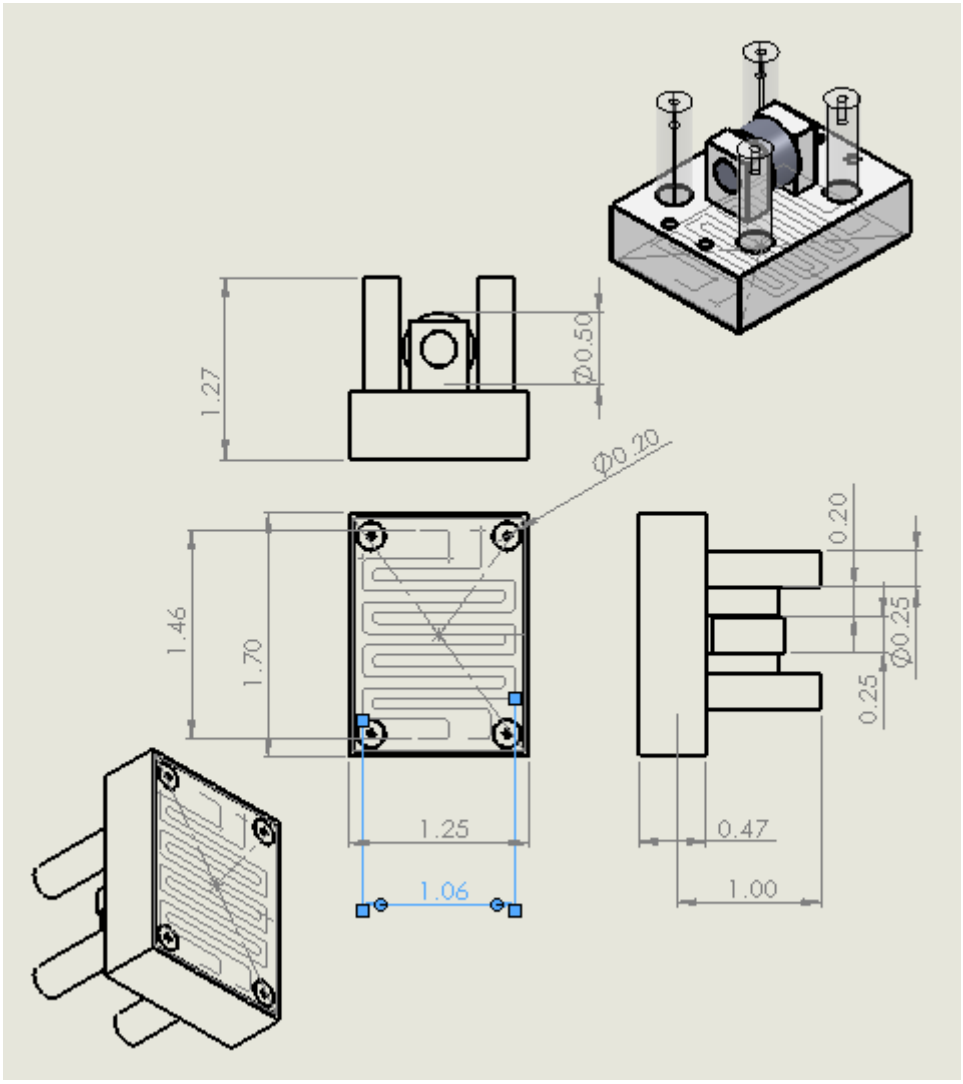

Figure 57: Heat Exchanger

B.3 Final Design

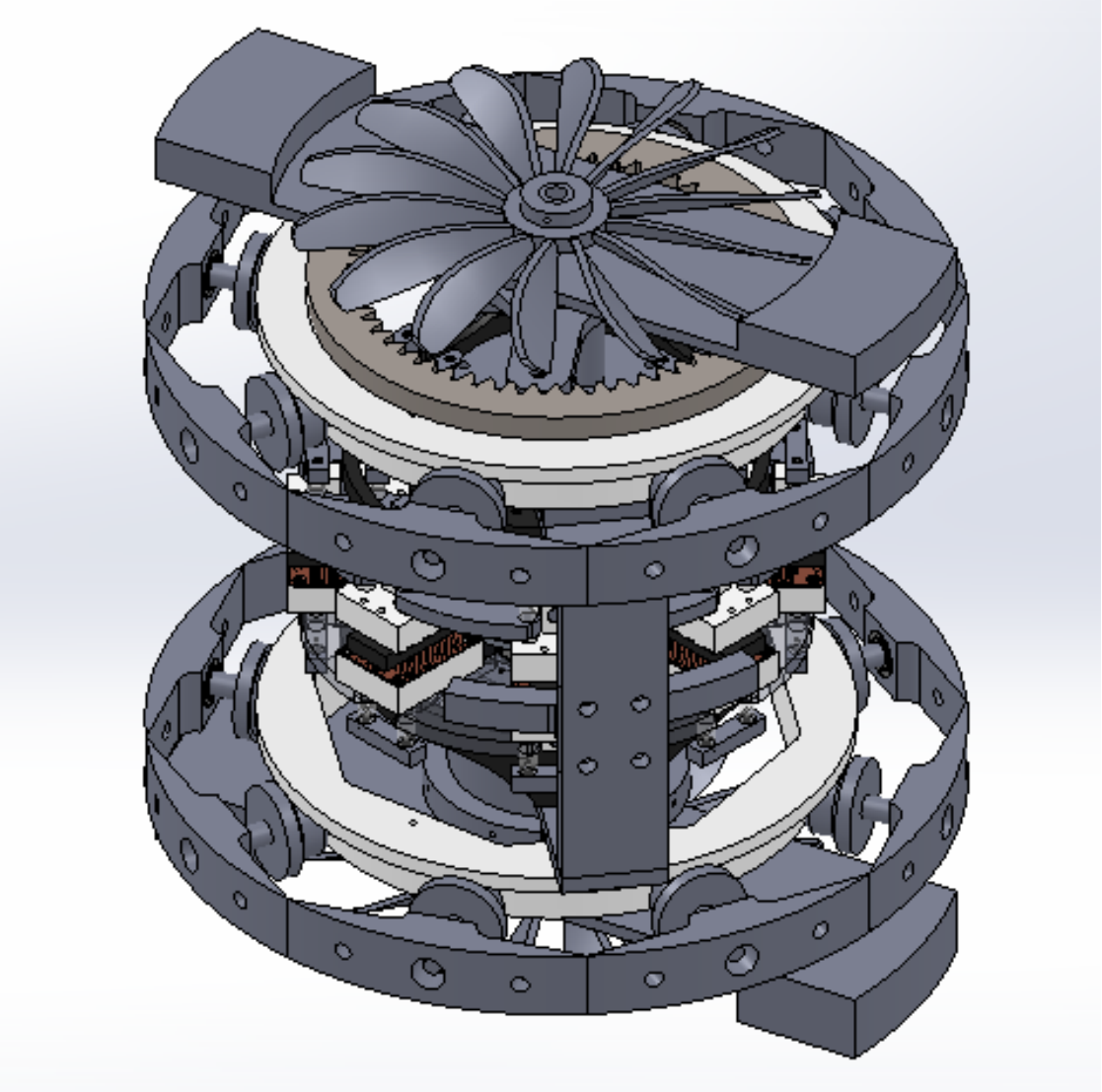

Figure 58: Magnetocaloric Material Test Bench